JOURNAL OF PROPULSION AND POWER
Vol. 19, No. 5, September–October 2003

Experimental Diagnostics for the Study of Combustion Instabilities in Lean Premixed Combustors

J. G. Lee* and D. A. Santavicca†
Pennsylvania State University, University Park, Pennsylvania 16802

An improved understanding of the mechanisms of unstable combustion in lean premixed combustors is essential to the development of stable gas turbine combustion systems. To obtain such understanding, detailed experimental studies of the phenomenology of unstable combustion are required. A number of experimental diagnostic techniques for characterizing unstable combustion and the underlying instability mechanisms are discussed. This includes techniques based on pressure, chemiluminescence emission, infrared absorption, and laser-induced fluorescence measurements. The techniques themselves are discussed briefly; however, the primary objective is to present and discuss results illustrating how these techniques can be used to characterize the mechanisms of unstable combustion, to gain an improved understanding of unstable combustion, and to develop strategies for suppressing unstable combustion in lean premixed gas turbine combustors.

Introduction

THE problem of unstable combustion in lean premixed combustors continues to be a critical issue limiting the development of stable low-emissions gas turbine combustors for propulsion and land-based power-generation applications. To develop combustors that are capable of stable operation over their entire operating range, an understanding of the mechanisms that initiate and sustain unstable combustion and their relative importance at different operating conditions is essential.

Unstable combustion refers to self-sustained combustion oscillations at or near the acoustic frequency of the combustion chamber, which are the result of the closed-loop coupling between unsteady heat release and pressure fluctuations. That heat release fluctuations produce pressure fluctuations is well known and well understood[1–4]; however, the mechanisms whereby pressure fluctuations result in heat release fluctuations are not. In lean premixed gas turbine combustion systems, it is generally considered that flame–vortex interaction[5,6] and feed system coupling[7–11] are the most important of these mechanisms. Flame–vortex interaction refers to the interaction between the flame front and vortices that are periodically shed at the entrance to the combustor. As the vortex passes through the flame front, the flame is stretched by the vortex. Depending on the rate at which the flame is stretched and the local equivalence ratio, this interaction can either increase the flame area and, hence, the rate of heat release, or it can lead to local extinction and as a result decrease the rate of heat release. Feed system coupling refers to a modulation of the fuel flow caused by pressure fluctuations in the nozzle and fuel delivery system. These fuel flow fluctuations result in equivalence ratio fluctuations that are convected from the nozzle into the combustor. If the equivalence ratio fluctuation arrives at the flame front in-phase with the pressure fluctuation, the resulting heat release fluctuation amplifies the oscillations, whereas, if the equivalence ratio fluctuation arrives at the flame front out-of-phase with the pressure fluctuation, the resulting heat release fluctuation damps the oscillations. In most instabilities, it is likely that both flame–vortex interaction and feed system coupling play a role and that their relative importance varies with operating conditions and combustor design.

To understand the role and relative importance of flame–vortex interaction and feed system coupling during unstable combustion, measurements must be made that characterize the mechanisms, the resulting instability, and the relationship between the two. Of particular importance are measurements of pressure, heat release, equivalence ratio, and flame structure fluctuations. This paper discusses a number of diagnostic techniques that have been used for making such measurements. Most of the techniques require optical access and, therefore, are limited to use in laboratory-scale combustors or in full-scale single-nozzle combustor test rigs where optical access is available. The purposes of this paper are to discuss the application of these techniques to the study of combustion instabilities and, in particular, to demonstrate how these techniques can be used to gain an improved understanding of the mechanisms of unstable combustion in lean premixed combustors. Note that, to date, these techniques have primarily been used to study the mechanisms of unstable combustion under limit-cycle conditions and that there have been very few studies of the mechanisms involved in the transition from stable to unstable combustion.

Pressure Measurements

There are a number of ways to detect and characterize unstable combustion. The most basic measurement is that of the dynamic pressure in the combustor. This measurement is typically made using high-frequency response (up to 250 kHz), water-cooled, piezoelectric pressure transducers. From a measurement of the combustor pressure vs time, the magnitude, phase, and frequency of the pressure fluctuations, as well as various statistical properties,[12,13] can be determined.

A typical pressure trace from a longitudinal-mode instability in a laboratory-scale, lean premixed combustor is shown in Fig. 1a, along with the corresponding frequency spectrum in Fig. 1b. This particular instability exhibits a peak-to-peak pressure fluctuation of approximately 2 psi at a frequency of 360 Hz with weaker pressure fluctuations at the second and third harmonics, that is, 720 Hz and 1080 Hz. Proper interpretation of such measurements requires knowledge of the mode of the instability, which determines the location of the nodes and antinodes of the pressure oscillation. The instability mode can be determined by measuring the pressure at several locations in the combustor.[14] For example, identification and characterization of a longitudinal mode requires a minimum of three transducers located along the length of the combustor, that is, at the entrance, exit, and halfway between. To identify transverse or circumferential modes, it is necessary to locate multiple transducers at specific circumferential positions.

Received 7 January 2003; revision received 23 June 2003; accepted for publication 26 July 2003.

*Senior Research Associate, Department of Mechanical and Nuclear Engineering.

†Professor, Department of Mechanical and Nuclear Engineering. AIAA Senior Member.

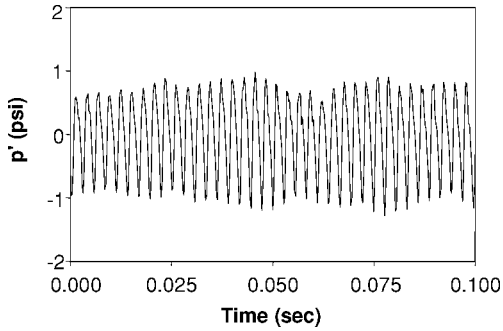

a) Time trace

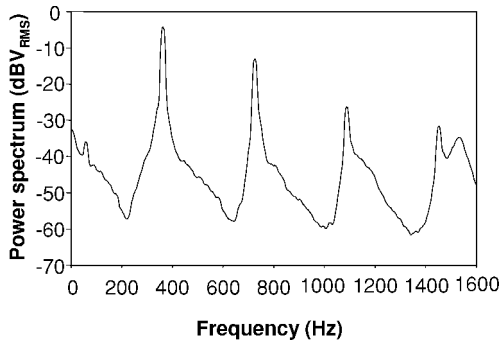

b) Power spectrum

Fig. 1 Typical pressure fluctuation during unstable combustion.

A simpler approach, which can sometimes be used to identify the mode, is to estimate the acoustic frequencies of the different modes, which are given by the speed of sound in the combustor divided by the corresponding dimension of the combustor, and to compare those to the measured frequency. If the acoustic frequencies of the different modes are well separated, one can often match the measured frequency to that of a specific mode and, thereby, identify the mode of the instability.

To measure accurately combustor pressure fluctuations, the pressure transducer should be flush mounted with the inner wall of the combustion chamber. In some combustors, however, the design of the combustion chamber does not allow for this, or there might be concerns about exposing the transducer to the high temperatures of combustion. In such cases it is necessary to isolate the transducer from the combustion chamber using a recess mount with a small-diameter passageway between the transducer and the combustion chamber. When the pressure transducer is mounted in this manner, it is important to account for the acoustic characteristics of the passageway because they can alter the amplitude and phase of the measured pressure signal.[14] Another consideration when making pressure measurements is that the interaction between the flame and the pressure wave results in a three-dimensional acoustic field in the vicinity of the flame. As a result, the pressure at the wall of the combustor, where it is often measured, can differ in amplitude and phase by as much as 20% from the pressure at the flame.[15,16]

Combustor pressure measurements are often combined with other measurements when characterizing unstable combustion. (Examples of such measurements are presented in the following sections.) When doing so, it is important to phase synchronize the measurements with the pressure oscillation, in which case it is usually necessary to filter electronically the pressure signal to eliminate higher harmonics and noise from the pressure signal. When using an electronic filter for this purpose, care must be taken to account for the phase delay introduced by the filter to synchronize correctly the two measurements.

In addition to measuring pressure fluctuations in the combustor, it is useful to simultaneously measure pressure fluctuations in the nozzle and the fuel line. These fluctuations result in fluctuations in the fuel flow rate, a phenomenon that was discussed earlier and that is referred to as feed system coupling.[7–11] Such measurements provide

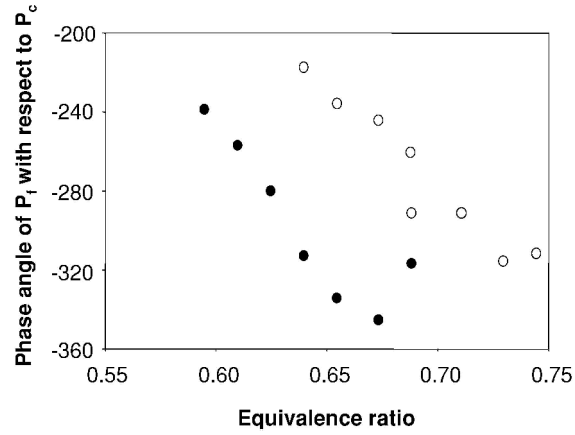

Fig. 2 Phase difference between fuel-line pressure and combustor pressure fluctuations vs equivalence ratio: ●, original length fuel line and ○, extended length fuel line.

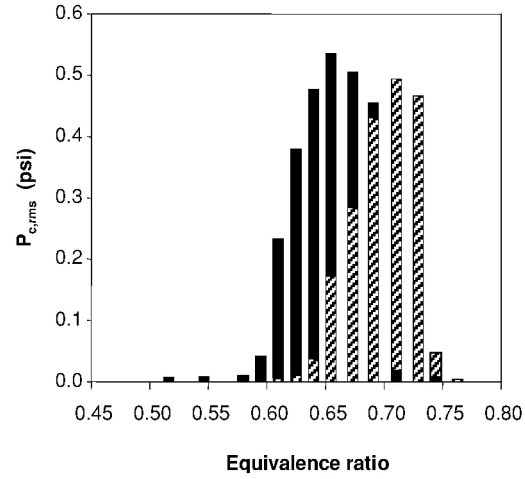

Fig. 3 RMS fluctuation in combustor pressure vs equivalence ratio: ■, original length fuel line; and ▨, extended length fuel line.

valuable information for assessing the role of feed system coupling as an instability driving or damping mechanism. They can also be used as a guide when attempting to modify the nozzle or fuel system geometry to alter the relative phase of the equivalence ratio and heat release fluctuations to suppress the instability. This has been successfully demonstrated in a single-nozzle research combustor[17] and a single-nozzle industrial nozzle,[18] resulting in attenuation of the pressure oscillation and a shift of the instability range. For example, Fig. 2 shows the phase difference between the pressure fluctuation in the combustor and the pressure fluctuation in the fuel line as a function of equivalence ratio for two different fuel line geometries.[18] The geometry change in this case involved decreasing the length of the fuel line between the fuel injector and an upstream choked orifice. The corresponding change in the stability characteristics of this combustor are presented in Fig. 3, where it is shown that the range of unstable combustion has shifted to higher equivalence ratios. Comparing Figs. 2 and 3 reveals that, with both fuel line geometries, the strength of the instability increases as the phase difference between the fuel line and the combustion chamber pressure fluctuations changes from approximately −250 to −300 deg, indicating the importance of feed system coupling and suggesting strategies for suppressing this instability.

Chemiluminescence Measurements

A second measurement that has proven extremely useful in characterizing unstable combustion in lean premixed combustors is that of the naturally occurring flame chemiluminescence. Chemiluminescence is the radiative emission from electronically excited species formed by chemical reactions.[19,20] The intensity of the

chemiluminescence emission is directly related to the concentration of the electronically excited species, which is determined by the competition between the chemical reactions that produce the excited species and collisional quenching reactions.

The strongest chemiluminescence emission in lean hydrocarbon flames is that due to CH*, OH*, and CO_2^* (The asterisk indicates an excited species.) Figure 4 shows a chemiluminescence emission spectrum measured in a laboratory-scale optically accessible lean premixed combustor, which is schematically shown in Fig. 5.[21] As shown, the chemiluminescence emission from CH* (431 nm) and OH* (309 nm) occur at distinctly different and relatively narrow wavelength intervals, whereas the CO_2^* chemiluminescence lies over a broad wavelength interval (350–600 nm) and overlaps the CH* and OH* chemiluminescence spectra. For diagnostic applications, there are several considerations to keep in mind when choosing between OH*, CH*, and CO_2^* chemiluminescence. One is that the CO_2^* chemiluminescence signal strength can be significantly increased over that of OH* and CH* chemiluminescence by using a very broad band filter, for example, $\Delta\lambda = 100$–200 nm, when detecting the chemiluminescence emission. The second is that, to detect OH* chemiluminescence, which occurs below 350 nm, ultraviolet-grade optics must be used. Last, elimination of the CO_2^* chemiluminescence from an OH* or CH* chemiluminescence measurement requires the added complexity of an independent measurement of the CO_2^* chemiluminescence background. As a result, most OH* and CH* chemiluminescence measurements that have been reported include a significant contribution due to CO_2^* chemiluminescence.

Measurements of the chemiluminescence emission from lean premixed flames have been used in numerous studies as an indicator of the location of the reaction zone and to infer local and overall heat release rates.[22–38] The rationale for such measurements is usually based on the experimental observation that, for a fixed equivalence ratio, the intensity of chemiluminescence emission from the entire flame, hereafter referred to as the overall chemiluminescence emission, increases linearly with the fuel flow rate, where the slope increases with increasing equivalence ratio.[22–26] This is shown in Fig. 6, which shows the overall CO_2^* chemiluminescence emission as a function of the fuel flow rate for a fixed equivalence ratio and inlet temperature. These results were obtained in the laboratory-scale optically accessible lean premixed combustor shown in Fig. 5.[21] The CO_2^* chemiluminescence was detected by imaging the entire flame onto a photomultiplier tube through a glass filter (BG-40), which transmits over the wavelength interval from 325 to 650 nm. The results shown in Fig. 6 indicate that the overall chemiluminescence intensity is a function of both the fuel flow rate, that is, the overall heat release rate, and the equivalence ratio. (This observation has important implications regarding the use of the overall chemiluminescence emission as a measure of the overall rate of heat release during unstable combustion, which will be discussed later.) The effect of equivalence ratio on the overall chemiluminescence emission is shown more clearly in Fig. 7, which is the overall chemiluminescence emission divided by the fuel flow rate vs equivalence ratio for a constant inlet temperature (650 K) and inlet velocity (67 m/s). These measurements were made in the same combustor described earlier. This result indicates that the overall chemiluminescence emission increases exponentially with equivalence ratio, which can be attributed to the exponential temperature dependence of the reaction rate for the formation of CO_2^* (Ref. 39).

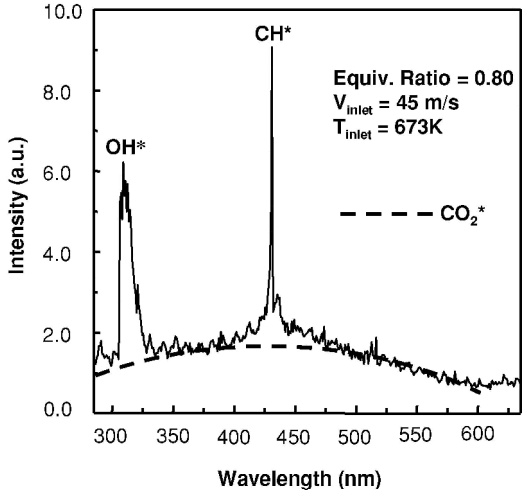

Fig. 4 Chemiluminescence emission spectrum from a lean premixed combustor operating at 100 kPa on natural gas at an equivalence ratio of 0.8 with an inlet temperature of 673 K.

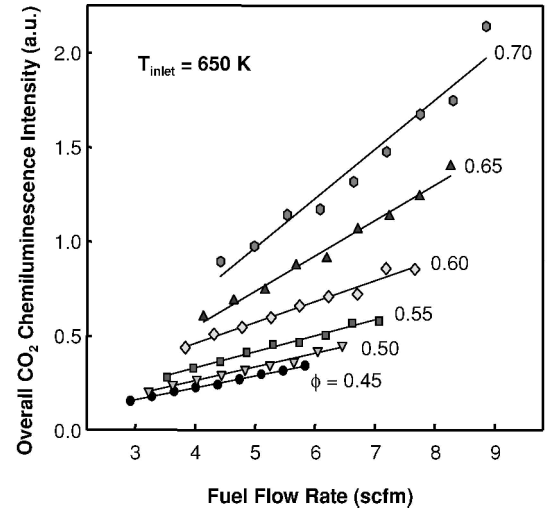

Fig. 6 Overall CO_2 chemiluminescence emission vs fuel flow rate.

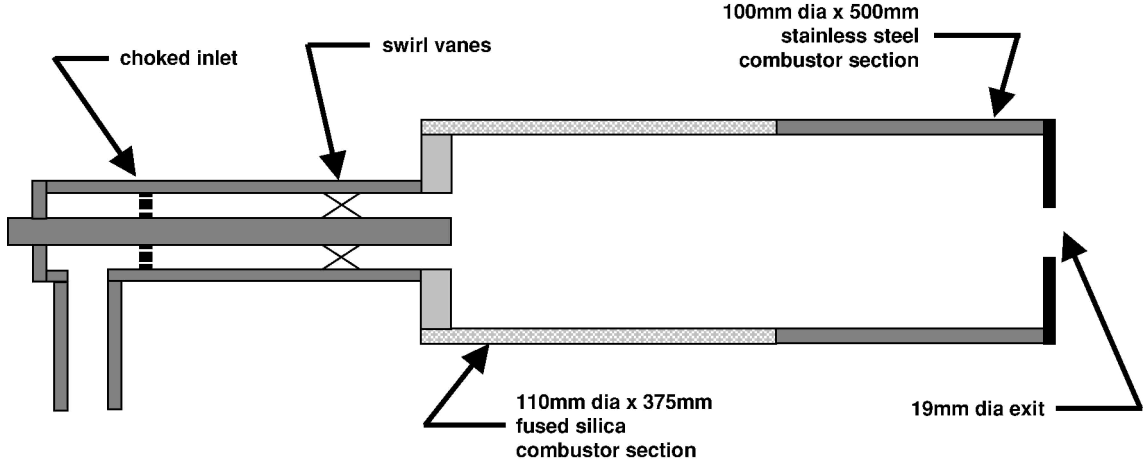

Fig. 5 Schematic of optically accessible lean premixed combustor.

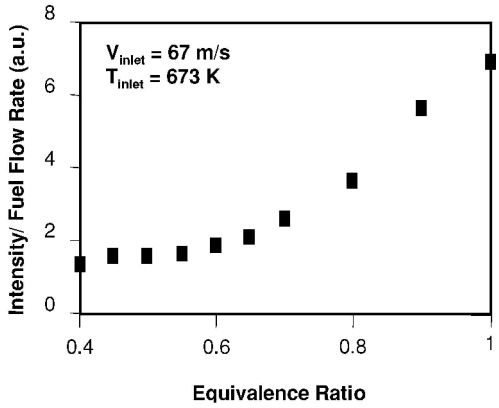

Fig. 7 Overall CO_2 chemiluminescence emission divided by fuel flow rate vs equivalence ratio.

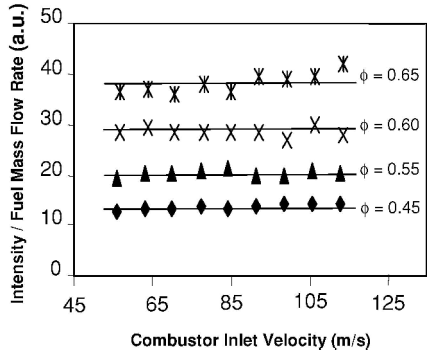

Fig. 8 Overall CO_2 chemiluminescence intensity divided by fuel flow rate vs combustor inlet velocity.

The fact that it is the flame temperature, and not the equivalence ratio per se, that affects the intensity of the chemiluminescence emission, is further evidenced by the observation that the overall chemiluminescence emission can be increased by increasing either the equivalence ratio or the inlet temperature.[21,39] Measurements in this same combustor of the overall OH* chemiluminescence and the overall CH* chemiluminescence also show a linear dependence on the fuel flow rate and an exponential dependence on equivalence ratio.[21] For these measurements, the OH* chemiluminescence was detected using a bandpass filter centered at 307 nm with a full width at half maximum (FWHM) of 10 nm, and the CH* chemiluminescence was detected with a bandpass filter centered at 430 nm and a FWHM of 10 nm.

In addition to the effects of fuel flow rate and equivalence ratio, some studies have shown that turbulence reduces the intensity of the overall chemiluminescence emission.[22,25] In tests conducted in the same lean premixed combustor already discussed (Fig. 5), however, such an effect was not observed. These results are shown in Fig. 8, which shows the overall CO_2^* chemiluminescence intensity divided by the fuel flow rate vs the combustor inlet velocity for constant values of equivalence ratio and a fixed inlet temperature of 650 K. As shown, the inlet velocity was increased by a factor of two, corresponding to a change in the Reynolds number from 9×10^3 to 1.8×10^4, with no apparent decrease in the overall chemiluminescence intensity.

To better understand the relationship between the rate of heat release and chemiluminescence emission, several studies involving detailed chemical kinetic calculations of lean premixed laminar methane–air flames have been conducted to investigate the relationship between the local rate of heat release, that is, the rate of heat release per unit flame area, and the local chemiluminescence emission, that is, the rate of chemiluminescence emission per unit flame area.[39–42] These studies have shown that CH*, OH*, and CO_2^* occur within the reaction zone, indicating that the location of the chemiluminescence emission can be used as an indicator of the location of the reaction zone. They have also shown that there is a correlation between the chemiluminescence emission from both OH* and CO_2^* and the local rate of heat release. An exception to both of these results, however, is in the case of extreme local strain or flame curvature, for example at cusps, where the calculations show that the chemiluminescence emission can effectively go to zero without extinction of the flame. The studies also indicate that most of the fuel goes through a reaction path that includes the formation of CO_2^*, suggesting that CO_2^* chemiluminescence should be a good indicator of the rate of heat release. Last, the studies show that the local rate of heat release $H_{R_{\text{local}}}$ and the local chemiluminescence emission I_{local} are affected by unsteady strain and flame curvature and that they increase exponentially with temperature, leading to a power law relationship between the local chemiluminescence emission and the local rate of heat release, that is,

$$I_{\text{local}} \propto (H_{R_{\text{local}}})^{\alpha}$$

where the exponent α is a positive number and depends on the flame temperature (as determined by the equivalence ratio, unburned gas temperature, dilution, and radiation losses) and on the effects of unsteady strain and flame curvature.[39]

To determine the relationship between the overall chemiluminescence emission I_{overall} and the overall rate of heat release $H_{R_{\text{overall}}}$, one must integrate the local values over the flame area, that is,

$$I_{\text{overall}} = \int_A I_{\text{local}}\, \mathrm{d}A_{\text{flame}}, \qquad H_{R_{\text{overall}}} = \int_A H_{R_{\text{local}}}\, \mathrm{d}A_{\text{flame}}$$

If the flame temperature, that is, the equivalence ratio, unburned gas temperature, dilution, and radiation losses, are constant and the effects of strain and flame curvature are negligible or constant, then I_{local}, $H_{R_{\text{local}}}$, and α are constant over the flame, which leads to the result that the overall chemiluminescence emission and the overall rate of heat release are proportional, that is,

$$I_{\text{overall}} = C H_{R_{\text{overall}}}$$

where the constant C depends on the flame temperature, that is, equivalence ratio, unburned gas temperature, dilution, and radiation losses, and the effects of strain and curvature. This result is consistent with the experimental results presented in Fig. 6, which show that for fixed equivalence ratio and inlet temperature the overall chemiluminescence emission increases linearly with fuel flow rate, that is, the overall rate of heat release, and that the slope depends on the equivalence ratio. Similarly, the results presented in Fig. 7, which show that the overall chemiluminescence emission divided by the fuel flow rate increases exponentially with the equivalence ratio, are also predicted by the detailed chemical kinetic calculations. Last, that the local chemiluminescence emission can be affected by unsteady strain and flame curvature is consistent with the observations that turbulence can reduce the overall chemiluminescence emission.

The relationship between the overall chemiluminescence emission and the overall rate of heat release, however, is more complicated if the equivalence ratio and/or the effects of strain and curvature vary over the flame area. This, for example, would occur in a partially premixed turbulent flame. In this case, the exponent α, in the equation relating the local chemiluminescence emission to the local rate of heat release, varies with location on the flame surface, which in turn affects the relationship between the overall chemiluminescence emission and the overall rate of heat release. To some extent, though, such variations are likely to average out such that the relationship between the overall chemiluminescence and the overall rate of heat release can be expressed in terms of the average equivalence ratio. Data supporting this are shown in Fig. 9, which shows the overall CO_2^* chemiluminescence emission, for constant inlet temperature (650 K), inlet velocity (84 m/s), and overall equivalence ratio conditions, vs a parameter referred to as "% premixed."[21] These measurements were made in the combustor illustrated in Fig. 5. In the 100% premixed case, the fuel and air are perfectly mixed, whereas in the 0% premixed case, there is a

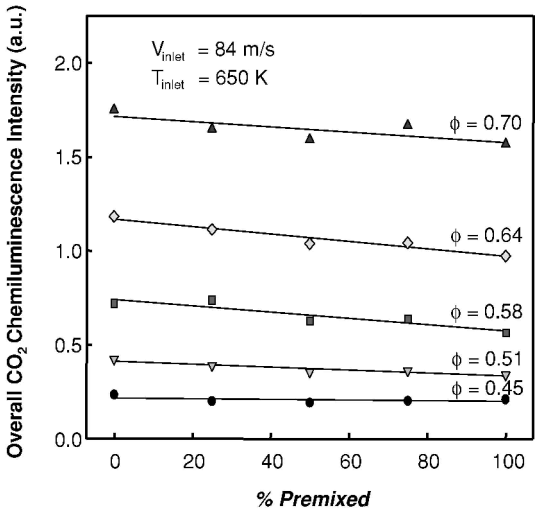

Fig. 9 Effect of incomplete fuel–air mixing on the overall CO_2^* chemiluminescence intensity.

gradient in the equivalence ratio across the annular mixing section, which, for example, varies from 0.3 to 0.9 for an overall equivalence ratio of 0.6. (Note that the fuel distribution measurement was made at the exit of the mixing section under cold-flow, noncombusting conditions.) The effect of incomplete mixing is to increase the overall chemiluminescence emission, as would be expected given the exponential dependence of chemiluminescence emission on equivalence ratio; however, the effect is small, that is, there is only a 10% increase in going from a 100% premixed to a 0% premixed condition.

The other factor affecting the overall chemiluminescence emission and the overall rate of heat release is, of course, the area of the flame. Any factors causing the flame area to change, for example, flame–vortex interaction, will result in a change in the overall chemiluminescence emission and the overall rate of heat release. Changes in the flame area will not alter the relationship between the overall chemiliuminescence emission and the overall rate of heat release, as long as the flame temperature and the effects of strain and curvature are constant. In other words, as the flame area changes, both the overall chemiluminescence emission and the overall rate of heat release will change in proportion to the area change. If, however, the effects of stretch and/or curvature change over the flame surface as the flame area changes, as might be expected during flame–vortex interaction, then the relationship between the overall chemiluminescence emission and the overall rate of heat release is likely to change as the flame area changes.

In general, the results of the detailed chemical kinetic studies support the use of chemiluminescence emission as a qualitative measure of the local and the overall rate of heat release in lean premixed flames; however, the studies also clearly indicate that even for qualitative applications such measurements should be interpreted with caution. (Another technique that has been proposed for making quantitative measurements of the rate of heat release is HCO fluorescence.[41,42] This technique is discussed in the section on laser-induced fluorescence measurements.)

In studies of unstable combustion, chemiluminescence emission has been used by numerous researchers to characterize temporal fluctuations in both the overall heat release[10,18,28,29,33,36–38] and the spatial distribution of the local heat release.[5,10,18,28–30,32,33,35,37] As the preceding discussion indicates, however, care must be taken when interpreting such measurements. For example, when making overall chemiluminescence measurements, it is important to realize that changes in the fuel flow rate and changes in the equivalence ratio independently affect the overall chemiluminescence emission, whereas only changes in the fuel flow rate affect the overall rate of heat release. This point can be illustrated by considering two combustors where the equivalence ratio at the inlet to the combustor is fluctuating, but for different reasons. In the first case, the equivalence ratio fluctuations are the result of fluctuations in the airflow rate, while the fuel flow rate is constant. Under these conditions, there will be fluctuations in the overall chemiluminescence emission, however, the overall rate of heat release will be constant. (This is not to be confused with the fact that the local rate of heat release, that is, the local flame speed, changes with local equivalence ratio. This is compensated for by changes in the flame area such that the overall rate of heat release remains constant.) In the second case, the equivalence ratio fluctuations are the result of fluctuations in the fuel flow rate, while the airflow rate is constant. Under these conditions, there will be fluctuations in the overall chemiluminescence emission that will be due in part to equivalence ratio fluctuations and in part to fuel flow rate fluctuations. In this situation, the chemiluminescence fluctuations overestimate the fluctuations in the overall rate of heat release. The only situation where the fluctuation in the overall chemiluminescence can be attributed solely to fluctuations in the overall rate of heat release is when the equivalence ratio is constant. In general, such conditions can only be achieved in a laboratory combustor, whereas in an actual combustor one would expect some degree of feed system coupling and as a result fluctuations in the equivalence ratio. Under such conditions, measurements of the overall chemiluminescence emission fluctuations without simultaneous measurements of the equivalence ratio fluctuations can potentially give misleading information about both the amplitude and phase of the overall heat release fluctuations.

There are also considerations when using chemiluminescence emission as a measure of the local rate of heat release. The most obvious is the fact that the chemiluminescence emission measurement is a line-of-sight measurement, that is, one measures the total emission integrated along the line of sight. This effect can be significantly reduced using an optical arrangement with a very short depth of field; however, this is at the expense of significantly reduced signal strength.[35] Another approach, if the flame is axisymmetric, is to use a deconvolution technique to reconstruct the two-dimensional emission field from line-of-sight chemiluminescence images. (This approach is discussed and illustrated later in this section.) It is important to realize that the two-dimensional chemiluminescence images obtained in this manner, however, do not actually represent the local chemiluminescence intensity, that is, on the scale of the flame thickness. Because of the line-of-sight nature of the chemiluminescence measurement, the two-dimensional chemiluminescence results effectively integrate over the local three-dimensional flame structure. In other words, the intensity of the chemiluminescence emission depicted in the two-dimensional chemiluminescence images, $I_{2\text{-D}}$, represents the product of the local chemiluminescence emission and the local flame area, that is,

$$I_{2\text{-D}} = I_{\text{local}} \cdot \bar{A}_{\text{local}}$$

where $\bar{A}_{\text{local}}$ is the flame area within a volume defined by the resolution of the line-of-sight measurement.

Similarly, one can define a two-dimensional rate of heat release $H_{R_{2\text{-D}}}$, which represents the product of the local rate of heat release and the local flame area, that is, $H_{R_{2\text{-D}}} = H_{R_{\text{local}}} \cdot \bar{A}_{\text{local}}$. Of interest is the relationship between the two-dimensional chemiluminescence emission and the two-dimensional rate of heat release. When the preceding equations are used, $I_{2\text{-D}} = (I_{\text{local}}/H_{R_{\text{local}}})\ H_{R_{2\text{-D}}}$. Using the power law relationship between the local chemiluminescence emission and the local rate of heat release, already discussed, gives the following relationship:

$$I_{2\text{-D}} = \left(H_{R_{\text{local}}}\right)^{\alpha - 1} \cdot H_{R_{2\text{-D}}} = C_{2\text{-D}} \cdot H_{R_{2\text{-D}}}$$

where $C_{2\text{-D}}$ depends on the local flame temperature and any factors that affect the flame temperature. Therefore, the intensity of the chemiluminescence emission shown in the two-dimensional chemiluminescence images is indicative of the two-dimensional rate of heat release; however, it can also change independently of the rate of heat release as a result of changes in the flame temperature and any factors that affect the flame temperature. As was the case with overall chemiluminescence measurements, the most likely concern would be in a partially premixed flame where variations in local

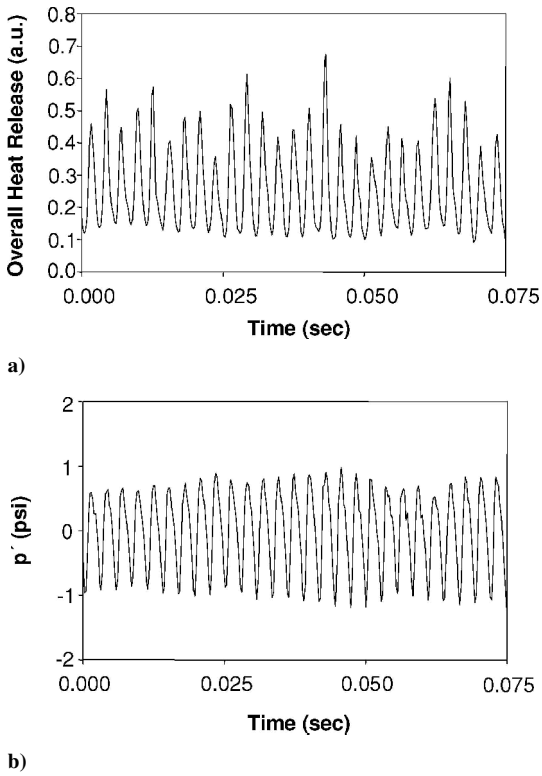

Fig. 10 During unstable combustion, simultaneous measurements of a) overall heat release fluctuations and b) combustor pressure fluctuations.

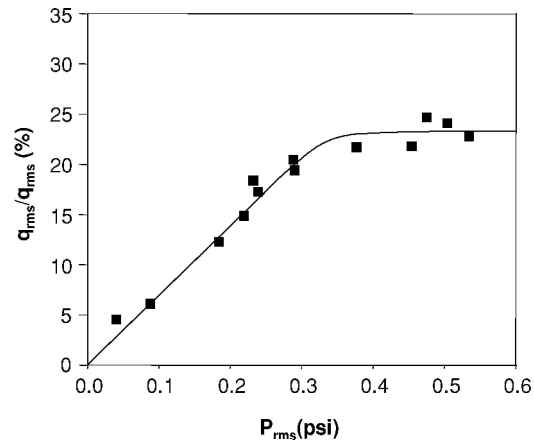

Fig. 11 RMS heat release fluctuation normalized by the average heat release vs rms pressure fluctuation at various unstable operating conditions.

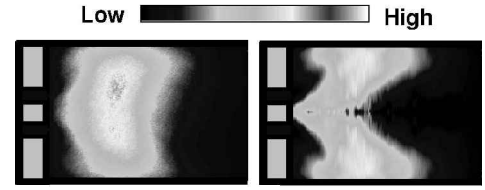

Fig. 12 Chemiluminescence a) line-of-sight integrated image and b) corresponding deconvoluted image.

equivalence ratio could lead to an inaccurate estimate of the local rate of heat release.

An example of a measurement of the overall heat release fluctuations during unstable combustion made in the optically accessible lean premixed combustor shown in Fig. 5 using CO_2^* chemiluminescence emission is shown in Fig. 10a, whereas the simultaneously recorded pressure fluctuation is shown in Fig. 10b. The overall CO_2^* chemiluminescence emission in Fig. 10a was measured by imaging the entire flame onto a photomultiplier tube through an appropriate bandpass filter as already described. Care must be taken when making such measurements to collect the chemiluminescence emission from the entire flame as to obtain an accurate indication of the total heat release rate and to avoid erroneous fluctuations due to the flame moving in and out of the field of view. Simultaneous measurements of the overall heat release rate and the pressure, such as shown in Fig. 10, can be used to determine the phase difference between the heat release and pressure fluctuations, which is related to the overall system damping and gain characteristics.[1] Such measurements also provide information on how the flame's heat release responds to pressure fluctuations. For example, Fig. 11 shows the rms overall heat release fluctuation normalized by the mean overall heat release (measured using CO_2^* chemiluminescence) vs the rms combustor pressure fluctuation during unstable combustion. These measurements were made in an optically accessible single-nozzle test rig equipped with a full-scale, industrial fuel nozzle (Solar Turbines Centaur 50) operating on natural gas at an inlet temperature of 660 K over a range of inlet velocities from 75 to 100 m/s and a range of equivalence ratios from 0.575 to 0.7. This result shows that the normalized heat release fluctuation increases linearly as the pressure fluctuation increases until it becomes saturated at high-pressure fluctuations, indicating that there is a nonlinear relationship between the pressure and heat release fluctuations during unstable combustion.[43,44] A more comprehensive assessment of the nonlinear response of lean premixed flames to pressure fluctuations can be obtained from forced response studies where the amplitude and relative phase of heat release fluctuations resulting from imposed pressure fluctuations over a range of frequencies and amplitudes are measured.[38]

Chemiluminescence emission can also be recorded using an intensified charge-coupled device (CCD) camera to obtain an image of the flame structure during unstable combustion that represents the spatial distribution of the flame's heat release. An example of such a measurement is shown in Fig. 12a, where a CO_2^* chemiluminescence image of the flame in a laboratory-scale lean premixed dump combustor (Fig. 5) operating on natural gas is presented. The gray scale shown above the image indicates the magnitude of the chemiluminescence intensity. The left-hand side of each chemiluminescence image shows the centerbody and the dump plane, as well as the location of the image within the 110-mm-diam quartz combustor. The direction of flow in this and all subsequent chemiluminescence images is from left to right. For this measurement, the image acquisition is phase synchronized with the pressure oscillation and a total of 30 individual images at that same phase angle are averaged to obtain the phase-averaged image shown in Fig. 12a. This image is a record of the line-of-sight integrated chemiluminescence intensity and, therefore, does not reveal the cross-sectional structure of the flame. If the flame is assumed to be axisymmetric, one can use a deconvolution procedure to reconstruct the two-dimensional flame structure, including onion-peeling, Abel transformation, and filtered backprojection methods.[45] The line-of-sight image shown in Fig. 12a was processed using an Abel deconvolution procedure. The resulting image, (Fig. 12b) reveals the two-dimensional structure of the flame that was not apparent in the original line-of-sight image.

A basic assumption of the deconvolution procedure is that the image is axisymmetric. Because the line-of-sight image in Fig. 12a is not perfectly axisymmetric, the upper and lower halves of the image were averaged to create an axisymmetric image before applying the Abel inversion. This procedure of creating an axisymmetric line-of-sight image is usually necessary; however, care must be taken when interpreting the resulting reconstructed images. If the line-of-sight images are reasonably axisymmetric, the insights gained from the reconstructed two-dimensional images usually outweigh the uncertainty associated with the axisymmetric approximation. Unfortunately there is no way to quantify this tradeoff; therefore, the reconstructed two-dimensional images must always be interpreted with care.

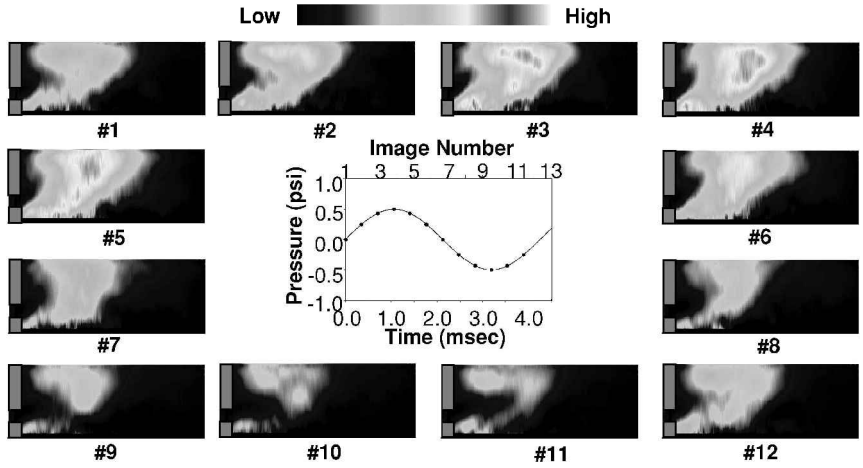

Fig. 13 Flame structure during one period of unstable combustion with a frequency of 235 Hz.

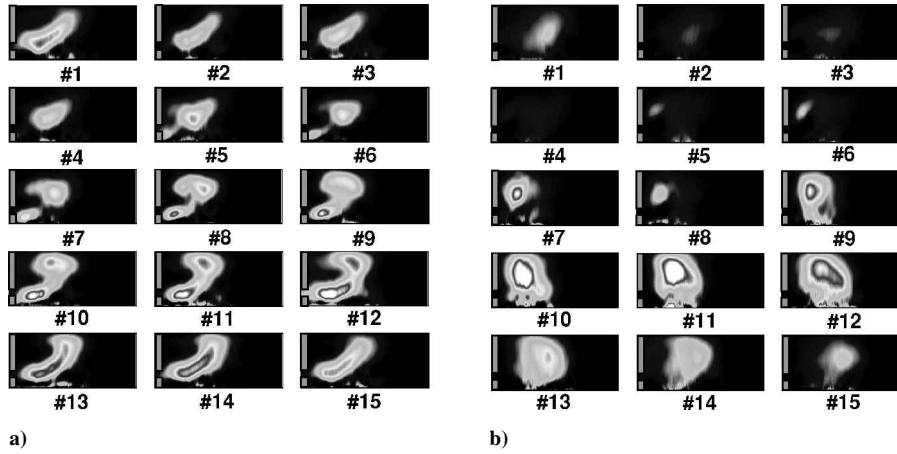

Fig. 14 Flame structure during one period of unstable combustion with a frequency of 350 Hz at two different operating conditions in the same lean premixed combustor.

Figure 13 shows a sequence of 12 phase-averaged two-dimensional CO_2^* chemiluminescence images recorded in increments of 30 phase-angle degrees during one period of a 235 Hz instability in the same laboratory-scale lean premixed dump combustor mentioned earlier. In this case the combustor was operating at 100 kPa, with an inlet temperature of 673 K, an inlet velocity of 45 m/s, and an equivalence ratio of 0.45. In addition, the exit of the combustor was not restricted (Fig. 5); hence, the marked change in the frequency of the instability compared to earlier results in this combustor. Note that only the upper-half of the flame is shown because the reconstructed images are axisymmetric. Again, to the left of each image is shown the location of the image relative to the combustor. Also shown in Fig. 13 is a plot of the combustor pressure vs time, measured at the dump plane, over one period of the instability with markers indicating when each of the images was recorded. The two-dimensional flame structure image sequence reveals the temporal evolution of the flame structure during the instability and provides insight regarding the phenomenology of the instability. For example, the images in Fig. 13 show a flame that is anchored on the centerbody and extends outward into the recirculation zone and all of the way to the wall of the combustor. The overall flame shape remains very nearly the same during the instability; however, there is a noticeable change in the overall intensity of the flame's heat release, indicating that minimum heat release, that is, images 9–11 (Fig. 13), occurs when the pressure is minimum. There is also a periodic break in the flame between where it is attached to the centerbody and the recirculation zone, which also occurs when the pressure and overall heat release are at their minimum levels.

Two flame structure image sequences are shown in Figs. 14a and 14b, which correspond to instabilities in the same lean premixed combustor (Fig. 5) and at the same operating conditions ($T_{\text{inlet}} = 623$ K, $V_{\text{inlet}} = 59$ m/s, and $\phi = 0.58$), except that the inlet fuel distribution is different. In Fig. 14a, the fuel and air are completely mixed before entering combustor, whereas in Fig. 14b, although the overall equivalence ratio is the same, the equivalence ratio increases with increasing radius across the annular outlet of the mixing section. Again, only the upper-half of the image is shown because the reconstructed images are axisymmetric. In both cases the instability frequency is approximately 350 Hz, and the phase-synchronized images are acquired in increments of 24 phase-angle degrees, giving a total of 15 images within one period, where each image is an average of 30 individual images acquired at a given phase angle. Both cases show evidence of flame–vortex interaction; however, the details of the interaction are noticeably different in the two cases. The flame in Fig. 14a appears to be wrapped around the vortex, resulting in stretching and contraction of the flame zone, whereas in Fig. 14b the flame appears to be contained within the vortex, exhibiting periodic extinction and reignition of the entire reaction zone.

Two-dimensional flame structure images, such as those shown in Figs. 13 and 14, reveal the location and intensity of the flame's heat release and its temporal evolution during one period of the instability. Combining this information with the measured pressure fluctuation, one can calculate the Rayleigh index distribution $R(x, y)$, which is given by the following equation:

$$R(x, y) = \frac{1}{T} \int_T p'(x, y, t) q'(x, y, t)\, \mathrm{d}t$$

where $q'(x, y, t)$ is the local heat release fluctuation determined from the two-dimensional flame structure images and $p'(x, y, t)$ is the local pressure fluctuation.[5,18,28–30,32,33,37] Because

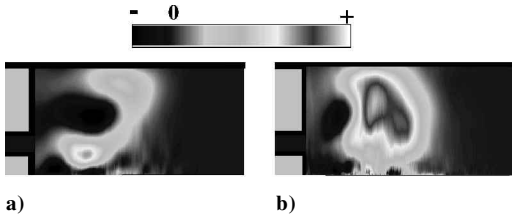

Fig. 15 Rayleigh index distributions corresponding to the unstable flames shown in Figs. 14a and 14b, respectively.

the wavelength of the pressure oscillation is often much greater than the length of the flame, the pressure in that case can be assumed to be spatially uniform over the region of heat release and, therefore, only a function of time.

The Rayleigh index is a measure of the correlation between the heat release fluctuation and the pressure fluctuation and, therefore, represents the strength of the coupling between the two. A positive Rayleigh index indicates that the heat release and pressure fluctuations are in-phase, in which case the heat release amplifies the pressure fluctuation. A negative Rayleigh index indicates that the heat release and pressure fluctuations are out-of-phase, and therefore, the heat release acts to damp the pressure fluctuation.

The Rayleigh index distributions corresponding to the two-dimensional flame structure images shown in Figs. 14a and 14b are presented in Figs. 15a and 15b, respectively, where the accompanying gray scale indicates the value of the Rayleigh index. The Rayleigh index distribution can be used to identify locations where the instability is amplified, that is, regions of positive Rayleigh index, and locations where the instability is damped, that is, regions of negative Rayleigh index, and thereby provide insight regarding the phenomenology of the instability. Figure 15a shows two damping regions, one in the recirculation zone behind the centerbody and the other in the recirculation zone downstream of the dump plane; there is a larger region of positive Rayleigh index along the shear layer between the dump plane and the centerbody recirculation zones. Fig. 15b shows a drastically different Rayleigh index distribution with a large region of positive Rayleigh index centered in the dump plane recirculation zone and a smaller damping region immediately downstream of the dump plane. A comparison of the locations of minimum and maximum Rayleigh index, that is, the locations of damping and gain, with the flame image sequence can provide insight as to the phenomenology of the instability and the role of the instability driving mechanisms.

Chemiluminescence emission measurements have also been shown to provide information and insights that can be used to optimize active combustion control systems employing modulated secondary fuel injection for the suppression of unstable combustion. For example, it has been shown that effective suppression of an instability can be achieved with less secondary fuel if the fuel is injected into the region of maximum damping indicated in the Rayleigh index distribution.[46] Chemiluminescence imaging can also be used to determine the optimum phase delay in active combustion control systems employing secondary fuel flow modulation.[46] When a pulse of secondary fuel is injected into a combustor, it produces a detectable modulation of the chemiluminescence emission, referred to as the flame response, which indicates when the secondary fuel reaches the flame front and burns. Using that signal as an indication of the heat release produced by the combustion of the secondary fuel pulse, one can calculate what is called the flame response Rayleigh index using the following equation:

$$\text{flame response Rayleigh index} = \frac{1}{T}\int_{t_0}^{t_0+T} p' q'_{\text{secondary}}\, \mathrm{d}t$$

where T is the period of the secondary fuel flow modulation, t_0 is the time delay between the pressure signal zero crossing and the secondary fuel valve trigger signal, p' is the measured pressure signal, and $q'_{\text{secondary}}$ is the flame response function. An example of the flame response function is shown in Fig. 16a.[46] In this case,

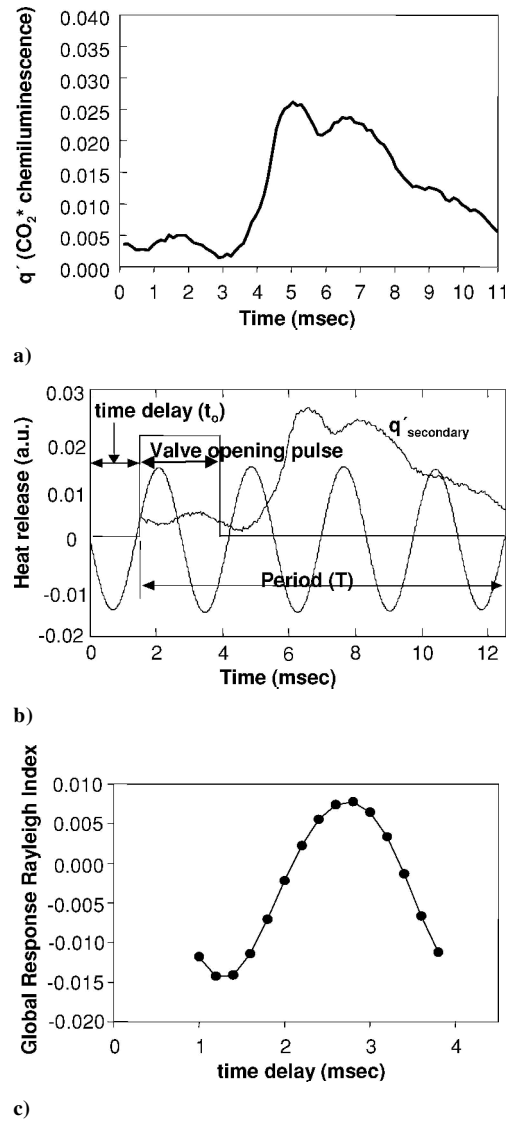

Fig. 16 Flame response a) function, b) function superimposed on unstable pressure trace, and c) Rayleigh index vs time-delay prediction.

subharmonic secondary injection is used, where the frequency of secondary fuel injection is one-fourth that of the instability. This is shown in Fig. 16b, where the flame response function is shown along with the pressure oscillation. Also shown in Fig. 16b is the control signal to the secondary fuel control valve and the time delay between that signal and the zero crossing of the pressure signal. The flame response Rayleigh index is a measure of the effect of the heat release due to the secondary fuel on the instability. If its value is positive, the secondary fuel acts to amplify the instability, whereas if it has a negative value, it acts to damp the instability, where the optimum phase delay corresponds to the case of maximum damping. The flame response Rayleigh index as a function of the time delay t_0 is plotted in Fig. 16c for the flame response function and pressure oscillation shown in Fig. 16b. According to this result, the time delay between the zero crossing of the pressure oscillation and the valve trigger signal for maximum damping is approximately 1.25 ms. This compares reasonably well with the experimentally determined delay time for maximum suppression of this instability, which is approximately 1 ms.

Infrared Absorption Measurements

Laser absorption techniques have been used to measure various flowfield parameters such as gas concentration, temperature, pressure, and velocity.[10,18,47–59] The basic technique involves passing laser light of known wavelength and intensity through the medium

of interest and measuring the attenuation of the light due to resonance absorption by specific atoms or molecules. The absorption process is described by Beer–Lambert's law, that is,

$$I/I_0 = 10^{-\int_0^l \epsilon c \, dx}$$

where I_0 is the intensity of incident light, I is the intensity of transmitted light, ε is the decadic molar absorption coefficient (square centimeter per mole), l is the absorption path length (centimeter), and c is the molar concentration of absorbing species (mole per cubic centimeter). The attenuation also depends on the temperature and pressure through changes in the absorption coefficient. The major limitation of this technique is that it is a line-of-sight measurement, that is, the measured attenuation is the result of the integrated absorption over the entire beam path and, therefore, is a measure of the average flowfield properties along the beam path.

The laser absorption measurement that has proven most valuable in the study of combustion dynamics is an infrared absorption measurement of hydrocarbon fuel concentration based on the fortuitous matchup between the 3.39-μm wavelength of the infrared helium–neon laser and a vibrational–rotational energy level transition in hydrocarbon molecules.[47,49] In this case, where the absorbing molecule is a stable species, the simplest procedure for making quantitative concentration measurements is to determine empirically the pressure and temperature dependence of the absorption coefficient. An example of this for methane is shown in Figs. 17a and 17b, where the normalized transmittance (I/I_0) vs temperature at a fixed pressure and vs pressure for values of constant temperature, respectively, are shown.[10] These measurements were made in a flow cell with a homogeneous methane–air mixture at known conditions. The 3.39-μm output from a He–Ne laser (3 mW) was used as a light source, and the transmitted light was detected using a thermoelectrically cooled indium–arsenide (InAs) detector. Once the normalized transmittance is known, the decadic molar absorption coefficient ε can be obtained from Beer–Lambert's law,

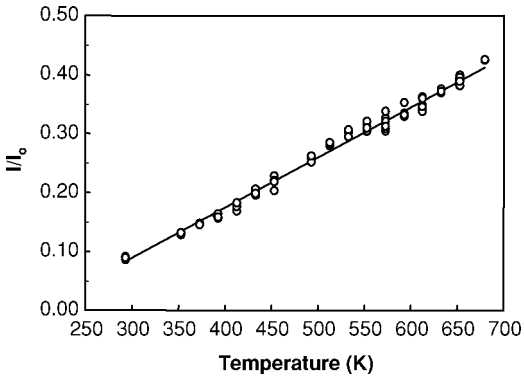

a) Temperature dependence

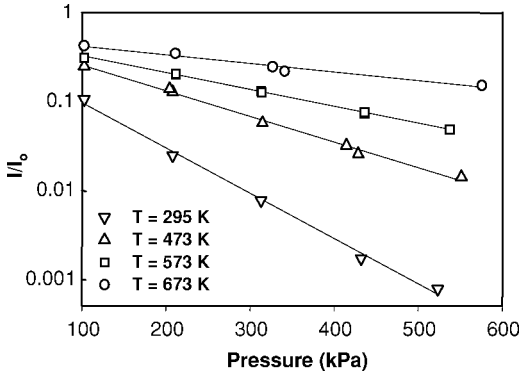

b) Pressure dependence

Fig. 17 Normalized transmittance I/I_0 of a 3.39-μm He–Ne laser beam through a homogeneous methane–air mixture.

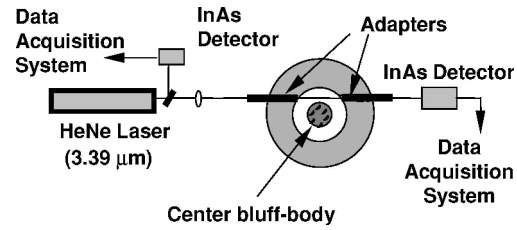

a) Front view

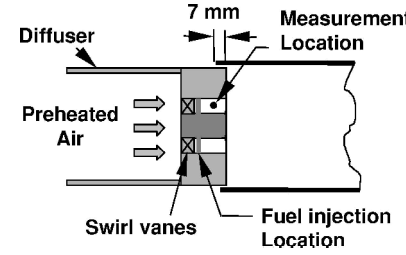

b) Side view

Fig. 18 Schematic setup for equivalence ratio measurements using infrared absorption.

that is,

$$\varepsilon = -(1/cl)\log_{10}(I/I_0)$$

With use of the data shown in Fig. 17, the following expression for the decadic molar absorption coefficient for methane as a function of pressure and temperature is obtained[10]:

$$\varepsilon = 84{,}737(P_0/P)(T/293\,\mathrm{K})\{C_1 + C_2[(P/P_0) - 1]\}$$

with $C_1 = -0.1131 + 1.1875(293\,\mathrm{K}/T)$ and $C_2 = 0.712 - 1.536\exp(-2.118 \times 293\,\mathrm{K}/T)$.

An important application of the infrared absorption technique in combustion instability studies is for measuring temporal fluctuations in equivalence ratio due to feed system coupling. The experimental setup for an infrared absorption measurement in a single-nozzle test rig equipped with a full-scale, industrial fuel nozzle (Solar Turbines Centaur 50) operating on natural gas is presented in Fig. 18.[18] As shown, the 3.39-μm laser beam passes through the annular mixing section in the injector, just upstream of the entrance to the combustor. This required a modification to the nozzle to provide two-sided optical access for the laser beam. Note that sapphire windows are required for transmission of the infrared beam. The actual measurement is of the normalized transmittance of the incident laser beam, that is, the ratio of the transmitted to the incident laser power. To convert this to equivalence ratio, an in situ calibration of the normalized transmittance vs the overall equivalence ratio is required. This involves making measurements over a range of equivalence ratios, without combustion, at fixed pressure and temperature. To use this calibration at other pressures and temperatures, one must account for the pressure and temperature dependence of the decadic molar absorption coefficient discussed earlier. In addition, the fact that the density changes with pressure and temperature must be accounted for because the absorption measurement actually measures fuel concentration not equivalence ratio.

Figure 19a shows the equivalence ratio vs time measured with the infrared absorption technique over one period of a 465-Hz instability in the combustor shown in Fig. 18. In this case, the combustor was operating on natural gas, at a pressure of 100 kPa with an inlet temperature of 658 K and an inlet velocity of 100 m/s. It is assumed that the temperature of the mixture in the nozzle is constant, and therefore, only fluctuations in the pressure are accounted for when converting the measured transmittance to equivalence ratio. This result clearly shows that feed system coupling is playing a significant role in this instability, resulting in peak-to-peak fluctuations in the equivalence ratio of approximately ± 0.05 about a mean of 0.65. The frequency spectrum corresponding to these fluctuations is shown

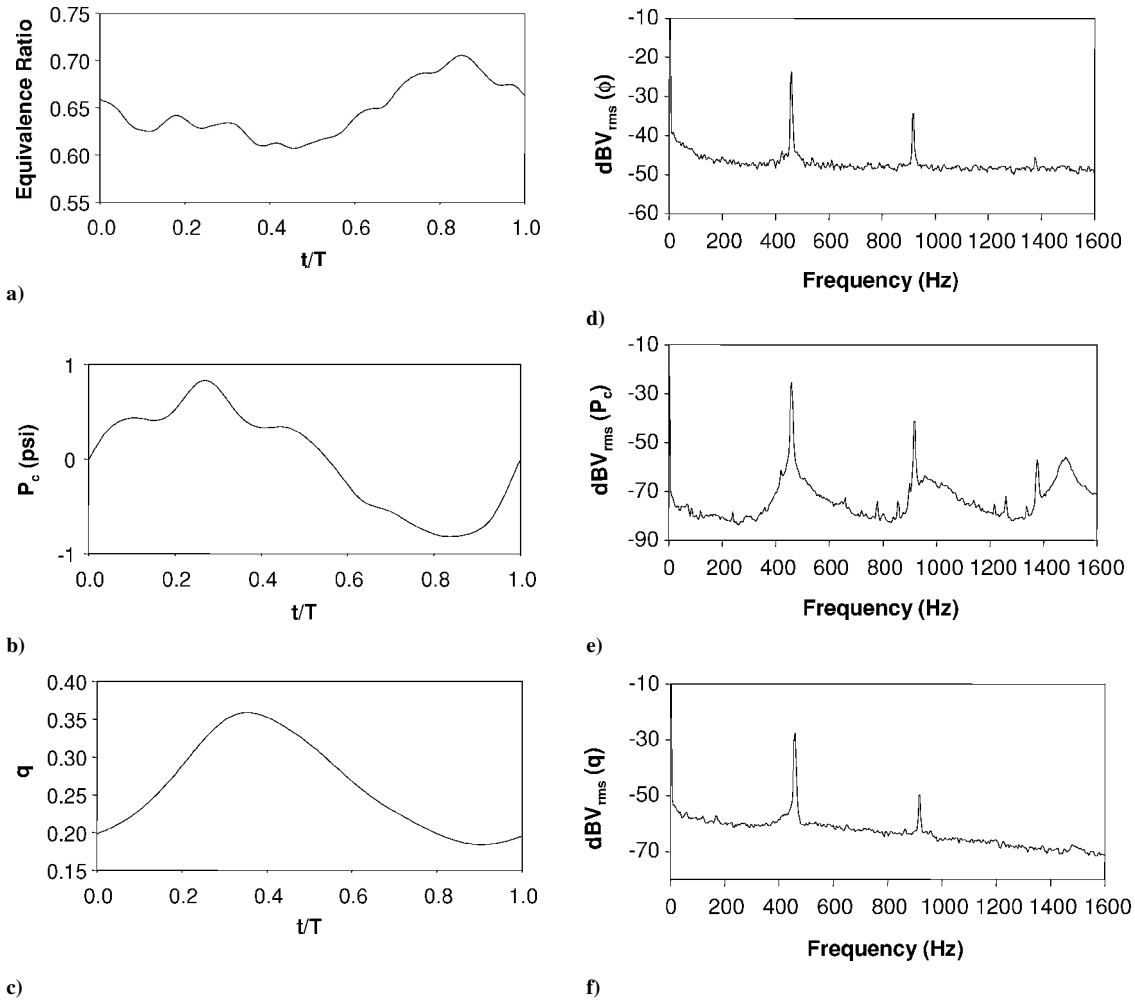

Fig. 19 Equivalence ratio, combustor pressure, P_c, and heat release, q, during one period, T, of unstable combustion: (a–c) time traces and (d–f) power spectra.

in Fig. 19d. The equivalence ratio fluctuations show a dominant frequency at 465 Hz, with weaker oscillations appearing at the higher harmonics. Shown in Figs. 19b and 19c are the phase-synchronized pressure and heat release measurements for this instability and in Figs. 19e and 19f the corresponding frequency spectra. It is clear that the dominant frequency of the equivalence ratio, pressure, and heat release fluctuations are the same, that is, 465 Hz. However, there are significant differences in the relative magnitude of the second-harmonic oscillations. Most noticeable is that there is only a 10-dB difference between the first and second harmonics of the equivalence ratio fluctuation, whereas there is a 23-dB difference between the first and second harmonics of the heat release fluctuations. This suggests that the flame, which is spatially distributed, acts to average out the higher frequency fluctuations in the equivalence ratio. Also of interest are the relative magnitudes of the pressure, equivalence ratio and heat release fluctuations, which for this instability are 3, 5, and 23% of the mean, respectively.

Last, the simultaneous pressure, heat release and equivalence ratio fluctuation measurements can be used to determine the phase delay or time lag between these processes. Of particular interest is the time lag between the equivalence ratio fluctuation and the heat release fluctuation because of its importance in assessing the role of feed system coupling. To estimate whether or not the equivalence ratio fluctuation produced by feed system coupling arrives at the flame front in-phase with the heat release fluctuation, one must estimate the convection time between the fuel injection location and the flame front. The most difficult part of the convection time to estimate is the time required for the fuel to travel from the entrance to the combustor to the flame front where the fuel burns. The phase delay or the time lag between the equivalence ratio and the heat release fluctuation shown in Figs. 19a and 19c is a direct measurement of that quantity.

The 3.39-μm helium–neon laser absorption technique has also been implemented in a fiber optic probe[50,55] and in a fast-response extraction probe.[57] The main advantage of this approach is that spatially resolved measurements are possible, that is, with a spatial resolution of the order of 1 mm. Such probes have been successfully used to measure spatial fuel distributions and equivalence ratio fluctuations in laboratory-scale and commercial single-nozzle lean premixed combustors.

Laser-Induced Fluorescence Measurements

The basic principal of the laser-induced fluorescence technique is that laser radiation is used to excite selectively an atomic or molecular species of interest to an upper electronic state via a laser absorption process.[60] The excitation process is followed by the spontaneous emission of a photon when the excited atom or molecule decays back to a lower energy level. The spontaneous emission is referred to as fluorescence, or in this case as laser-induced fluorescence, and its intensity can be related to the number density of the species of interest. To quantify the relationship between the fluorescence intensity and the number density of the absorbing species, one must account for the energy level population distribution of the absorbing atom or molecule and for collisional quenching and redistribution effects. For certain molecules, such as OH and CH, and with the selection of an appropriate excitation/detection scheme, it has been shown that the fluorescence signal is directly proportional to the concentration of the absorbing species.[61] Similarly, excitation/detection schemes have been developed for certain molecules that allow for the determination of the temperature.[62] In the case of stable species, these effects can be accounted for by simply calibrating the fluorescence intensity vs number density of the fluorescing species as a function of temperature and pressure. When calibrating

a fluorescence measurement, the overall composition should be approximately the same as in the actual measurement because collisional quenching is dependent on composition. Note, however, that quantitative fluorescence measurements are not always necessary and that useful information can often be obtained from qualitative measurements that provide a relative measure of the number density, or in some cases, only indicate the location of the species of interest.

At low laser excitation irradiance, the fluorescence signal S_f (joules per square centimeter) can be related to the mole fraction of the fluorescence seed, χ_{abs}, by the following equation:

$$S_f \propto (E/h\nu)[\chi_{\text{abs}}(P/T)]\sigma(\lambda, T)\phi(\lambda, P, T)$$

where E is the laser irradiance (joules per square centimeter), h is Planck's constant, ν is the laser frequency, χ_{abs} is the molar concentration of the fluorescence species, $\sigma(\lambda, T)$ is the molecular absorption cross section of the fluorescence species, and $\phi(\lambda, P, T)$ is the fluorescence quantum yield. In this equation, it is assumed that the effect of gas composition on the fluorescence yield is constant. For a fixed excitation wavelength and under isothermal and isobaric conditions, the fluorescence signal is only proportional to the mole fraction of the fluorescence seed. However, in flows where the temperature and pressure are changing, the effect of the energy level population distribution and of collisional quenching and redistribution on the absorption cross section and the fluorescence quantum yield, and therefore the fluorescence signal, must be accounted for, as discussed earlier.

Laser-induced fluorescence can be used to make point measurements with submillimeter spatial resolution or to make two-dimensional measurements, also referred to as planar laser-induced fluorescence (PLIF) measurements.[63,64] In the former case, the laser beam is focused with a spherical lens to a small diameter beam waist, and the fluorescence signal is detected by imaging the beam waist through an aperture onto a photomultiplier tube. In the latter case, the laser beam passes through a combination of cylindrical and spherical lenses to produce a thin laser sheet, and the resulting fluorescence signal is detected by imaging a portion of the laser sheet onto an intensified CCD camera. In both cases, an appropriate interference filter is used to isolate and selectively detect the desired fluorescence wavelengths. The fluorescence signal strength for gas-phase fluorescence measurements is typically very low, requiring the use of high-power pulsed lasers; however, depending on the fluorescence species and its concentration, single-pulse measurements are often possible. Unfortunately, high-power pulsed lasers operate at relatively low pulse rates, that is, typically 10–20 Hz; therefore, this technique does not provide a continuous measure of the fluorescence species concentration. However, for periodic phenomena, such as unstable combustion, the measurements can be phase synchronized with the instability and the periodic behavior reconstructed.

A useful application of laser-induced fluorescence in the study of combustion dynamics is for characterizing fuel–air mixing. This is an important measurement because both the temporal and spatial fuel distribution can have a significant effect on the stability characteristics of the combustor.[30] Many fuels of interest, however, are not well suited for fluorescence measurements, so that a common approach is to seed the fuel with a small amount of a fluorescence seed, where the concentration of the fluorescence seed, as measured by the fluorescence technique, is assumed to be an indicator of the fuel concentration. An advantage of using a fluorescence seed is that its concentration can be controlled. In addition, a fluorescence seed can be selected that has optimum physical and spectroscopic properties, making quantitative equivalence ratio measurements possible. Various species have been employed as fluorescence seeds for fuel–air mixing studies and detailed information on their fluorescence characteristics can be found in Refs. 65–70. A number of factors must be considered when selecting the fluorescence seed for characterizing mixing, including boiling point, autoignition temperature, absorption and fluorescence characteristics, mass diffusion coefficient, cost, toxicity, etc. For gaseous fuels, acetone is commonly used as a fluorescence seed because of its low boiling point (50°C at

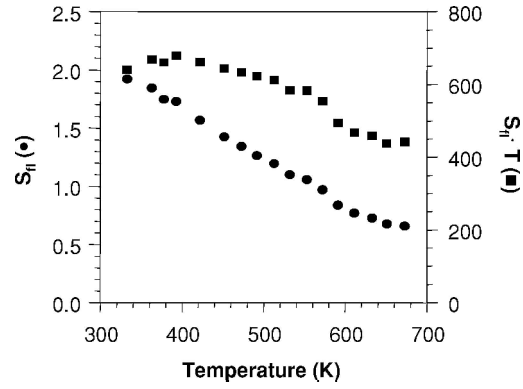

a) Temperature dependence

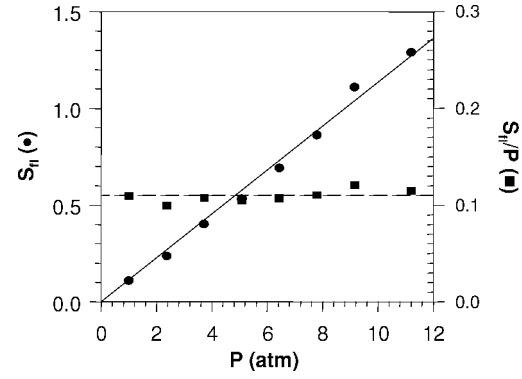

b) Pressure dependence

Fig. 20 Acetone LIF signal with 266-nm excitation.

1 atm) and high vapor pressure (184 torr at 20°C), which allows for easy seeding and high seed density. The spectroscopic characteristics of acetone are also well known. It absorbs over a broad range of wavelengths (225–320 nm) with maximum absorption between 270 and 280 nm. The fluorescence emission is broadband in the blue (350–550 nm) and short lived ($\tau \approx 4$ ns), with a fluorescence efficiency of 0.2% (Refs. 67–70).

Because acetone is a stable species, the effects of pressure and temperature on the absorption cross section and the fluorescence yield are best accounted for empirically. Figures 20a and 20b show the effect of temperature and pressure, respectively, on the acetone fluorescence signal with 266-nm excitation, that is, the fourth-harmonic output of a Nd:YAG laser. Figures 20a and 20b each show two curves. The solid circles are the actual measurements, whereas the solid squares have been corrected to constant number density. The measurements were made in a flow cell with the volume fraction of acetone fixed at 1%; therefore, changes in pressure and temperature also affect the fluorescence signal as a result of changes in the density. The actual measurements show that the fluorescence signal decreases with increasing temperature and increases with increasing pressure. After changes in density are corrected for, however, it is found that the fluorescence signal is independent of pressure, and it decreases with increasing temperature. Knowledge of the effect of pressure and temperature on the fluorescence signal, independent of their effect on density, is critical to the proper interpretation of fluorescence measurements. The temperature and pressure dependence of acetone laser-induced fluorescence using different excitation wavelengths may be found in Refs. 67–70.

Acetone PLIF was used to measure the fuel distribution in a natural gas-fueled laboratory-scale dump combustor, which is shown schematically in Fig. 21a.[71] This particular combustor was used in a study of the effect of combustor inlet fuel distribution on combustion stability and emissions and, hence, has the unique capability of allowing for systematic variation of the fuel distribution. This is accomplished by injecting the fuel at one or more of three injection locations, labeled 1–3 in Fig. 21a. For the acetone fluorescence measurements, the fuel is replaced with air to which 0.5%, by volume,

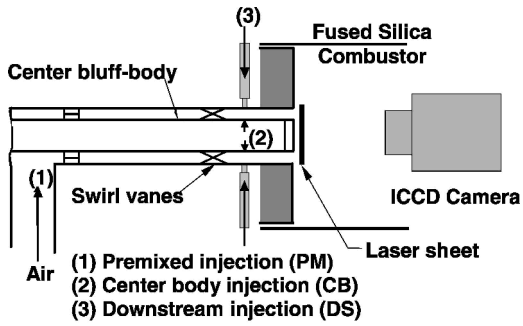

Fig. 21a Side view of the optically accessible axial dump combustor and schematic of PLIF setup.

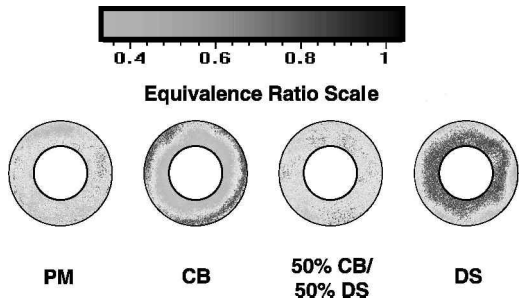

Fig. 21b Processed acetone PLIF images.

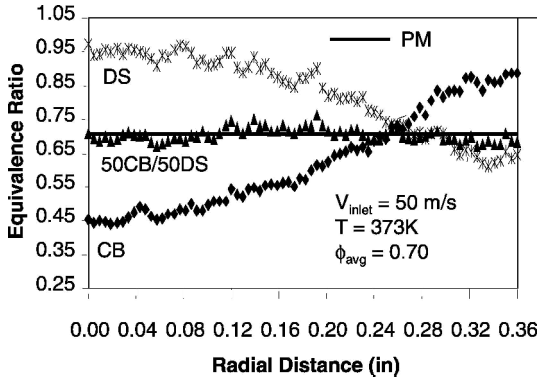

Fig. 21c Equivalence ratio distribution over the annular mixing section at the inlet of the combustor.

of acetone is added. (Therefore the measurements are made without combustion.) To ensure complete vaporization of the acetone, it is injected into the air using a spray nozzle, and the air is preheated to 100°C. Also note that, in the case of injection locations 2 and 3, the flow rate of the simulated fuel was set to match the momentum flux of the actual fuel jet.

The excitation source is the fourth-harmonic (266-nm) output of a pulsed Nd:YAG laser, with a laser pulse energy and duration of 40 mJ/pulse and 7 ns, respectively. The laser beam is formed into a 0.5 mm thick by 40 mm high sheet, which is positioned approximately 1 mm downstream of the dump plane across the exit of the annular mixing section. The fluorescence signal is recorded using an intensified CCD camera positioned downstream of the combustor, perpendicular to the laser sheet. Background noise subtraction and a uniform field correction are applied to each of the acetone PLIF images. In addition, the images are corrected for pulse-to-pulse fluctuations in laser energy. Figure 21b shows the processed images for four different fuel distributions, where only the fuel distribution across the annular mixing section is shown and the equivalence ratio values are indicated by the accompanying gray scale. These results are averages of 30 individual images and, therefore, represent the average fuel distribution. In all four cases, the overall equivalence ratio is the same, that is, 0.7, as are the combustor inlet velocity

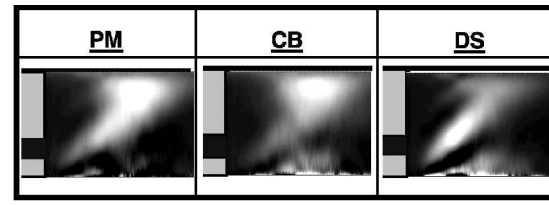

Fig. 22 Effect of inlet fuel distribution on flame structure for PM, CB, and DS fuel distributions of Fig. 21.

(50 m/s), inlet temperature (373 K), and pressure (100 kPa). In the premixed (PM) case, the fuel and air are premixed well upstream of the combustor. In this case, the fuel distribution is expected to be perfectly uniform. In the centerbody (CB) case, all of the fuel is injected through holes in the centerbody at a location approximately 25 mm upstream of the dump plane, that is, location 2. In this case, the fuel penetrates to the outer wall of the mixing section resulting in fuel-rich conditions along the outer wall and fuel lean conditions along the centerbody. In the downstream (DS) case, all of the fuel is injected through holes in the outer wall of the mixing section at a location approximately 25 mm upstream of the dump plane, that is, location 3. In this case, the fuel penetrates to the centerbody, resulting in fuel-rich conditions along the centerbody and fuel-lean conditions along the outer wall of the mixing section. Also note that there is evidence of the effect of the six-vane swirler on the fuel distribution in the DS image shown in Fig. 21b. Last, in the 50%CB/50%DS case, half of the fuel is injected through the holes located in the centerbody, location 2, and half is injected through the holes in the outer wall of the mixing section, location 3. The resulting fuel distribution is very uniform. These results are further quantified by calculating an average radial fuel distribution for each case. This is an average of the radial fuel distribution over 12 radial profiles spaced 30-deg apart around the axis of the combustor. These results are presented in Fig. 21c.

Figure 22 shows the CO_2^* chemiluminescence flame structure images corresponding to the PM, CB, and DS fuel distributions shown in Fig. 21. Note that the velocity, temperature and overall equivalence ratio were the same for all three cases and the combustor was stable at these conditions. In the PM case, the flame is anchored on the centerbody and extends outward all the way to the wall of combustor. For the CB case, there is a noticeable shift in the most intense region of the flame toward the outer wall of the combustor, which is consistent with the fact that the fuel concentration is greatest away from the centerbody, whereas for the DS case the most intense region of the flame has moved closer to the centerbody, where the fuel concentration is greatest. The fuel distribution also had an effect on the stability characteristics, that is, with PM injection, combustion was stable at low inlet velocities, but became unstable as the inlet velocity increased. In contrast, with CB injection, the reverse was true, that is, combustion became unstable as the velocity was decreased. Because velocity was found to have little effect on the fuel distribution, it can be argued that differences in the susceptibility of the different flame shapes to changes in velocity explain these results.

In combustors that do not have the optical access required for an acetone PLIF measurement, it is possible to use a fiber optic probe for making point measurements of the equivalence ratio and, thereby, determine the fuel distribution. A fiber optic laser fluorescence equivalence ratio probe has been developed and successfully used for this purpose.[72] The overall diameter of the probe is 16 mm ($\frac{5}{8}$ in.), and the length can be made to accommodate different combustors. The probe consists of a stainless steel, water-cooled jacket, inside of which are mounted two fused silica optical fibers, one for transmitting the laser beam and the other for transmitting the collected fluorescence signal. The measurement volume, which is approximately 1 mm in diameter and 3 mm in length, is located 25 mm from the side of the probe and faces upstream. This probe has been used to measure spatial and temporal fuel–air distributions in a number of industrial and research gas turbine combustor facilities at combustor pressures up to 10 atm and inlet temperatures up to 673 K, both with and without combustion.

Another application of laser-induced fluorescence is the use of HCO fluorescence to measure the rate of heat release. Although this technique has not been used to measure either local or overall rates of heat release in lean premixed gas turbine combustors, it is often mentioned as an alternative to the chemiluminescence technique and, therefore, warrants discussion. Two advantages of the HCO fluorescence technique, as compared to the chemiluminescence technique, are that the HCO mole fraction has been shown to be an accurate indicator of the flame's heat release, even in the presence of unsteady strain and flame curvature, and that the fluorescence measurement is spatially resolved.[41,42] The HCO fluorescence measurement, however, also has a number of disadvantages compared to the chemiluminescence technique. First, it requires both a laser and a detector, whereas the chemiluminescence technique requires only a detector. Second, it requires two-sided (90-deg) optical access, whereas the chemiluminecence technique only requires optical access from one direction. Third, the measurement rate is at best 20 Hz due to the limited pulse rate of the required laser system, whereas chemiluminescence measurements can be made continuously. Fourth, because the HCO fluorescence signals are very weak, it is unlikely that two-dimensional fluorescence measurements with adequate signal to noise will be possible over typical combustor dimensions. For these reasons, the chemiluminescence technique, although it only provides a qualitative measure of the rate of heat release, is a more viable approach for measuring heat release rates in lean premixed combustor experiments.

Last, another application of the laser-induced fluorescence technique is the use of OH PLIF to obtain detailed two-dimensional flame structure measurements during unstable combustion.[73–76] The reaction zones in lean premixed combustors can be expected to be predominantly in the so-called wrinkled laminar flame regime,[77–79] with the exception of conditions that are susceptible to local extinction, for example, regions of high strain and/or curvature, particularly near the lean limit. In the wrinkled laminar flame regime, the leading edge of the reaction zone, that is, the flame front, is characterized by a steep gradient in OH concentration. However, because OH is relatively long lived, it persists well into the high-temperature products downstream of the flame front.[61] The location of the steep gradient in OH concentration can be used as an indicator of the location of the reaction zone or flame front. Because OH PLIF signal strengths are typically strong, single-shot measurements are possible, which provide a detailed space- and time-resolved map of the two-dimensional flame structure.

An OH PLIF image from the laboratory-scale dump combustor in Fig. 5 is shown in Fig. 23a, where only the upper-half of the combustor is shown.[73,74] This is a single-shot image acquired at a particular phase angle during unstable combustion. It clearly shows that the flame is anchored on the centerbody. It also shows that there is a well defined and highly wrinkled flame front, indicating that combustion is occurring in the wrinkled laminar flame regime.[77] Last, there is clear evidence of the interaction between the flame front and the vortex, which is shed from the dump plane shoulder. Of particular interest is the effect of this interaction on the area of the flame because the flame area is directly related to the flame's rate of heat release.

The first step in calculating the flame area is determining the location of the flame front. This involves correcting the images for shot-to-shot laser energy variations, background noise, and laser sheet nonuniformity. Because there is a marked increase in OH concentration at the leading edge of the flame front, its location can be readily determined by applying a threshold to the corrected image. This threshold was not based on the magnitude of the OH fluorescence intensity, as is often done, but rather on the magnitude of the local gradient of the OH intensity.[73,74] This was done to avoid mistakenly identifying as a flame front the boundary between combustion products and unburned reactants, which result from the mixing of products and reactants in the recirculation zone of the dump combustor. The flame front determined by this threshold procedure from the OH PLIF image shown in Fig. 23a is shown in Fig. 23b. Once the flame front is determined, the total flame area is calculated by revolving the flame front around the centerline of the combustor.

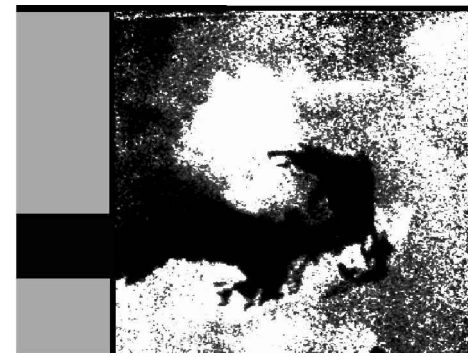

a) Normalized OH PLIF image

b) Thresholded flame surface

Fig. 23 Flame surface area calculation procedure.

An assumption in this calculation is that the flame front determined from the OH PLIF image is representative of the flame front at other cross sections of the flame. In addition because the OH PLIF image is a single-shot image, one must calculate the area for a number of such images from which an average flame area can be determined.

To understand the role of flame area changes during unstable combustion, it is necessary to obtain OH PLIF images at various times during one period of the instability. The image acquisition rate of the OH PLIF technique, however, is considerably less than typical instability frequencies. Therefore, it is necessary to reconstruct the image sequence by obtaining images at different phase angles from different cycles. Figure 24 shows a sequence of flame fronts determined from single-shot OH PLIF images over one period of a 378-Hz instability. These measurements were made in the laboratory combustor referred to earlier, operating on natural gas at an equivalence ratio of 0.9 with an inlet velocity of 59 m/s and temperature of 623 K. These results clearly show the evolution of the interaction between the flame front and the vortex and the resulting changes in the flame length. Five single-shot OH PLIF images were acquired at each phase angle, the flame area was then calculated for each image using the procedure already described, and an average flame area at each phase angle was calculated. The resulting flame area vs phase angle over one period of the instability is plotted in Fig. 25, along with the measured overall heat release fluctuation, that is, the overall CO_2^* chemiluminescence intensity fluctuation. In this case, the area and heat release fluctuations are very nearly in-phase, indicating that flame area changes due to flame vortex interaction plays an important role in this instability. Results such as these provide valuable insight regarding the phenomenology of unstable combustion and can be used to provide guidance for the development of reduced-order models of unstable combustion.[44]

Detailed two-dimensional OH flame structure measurements can also be used to calculate the local flame surface density, which is a measure of the local reaction rate in turbulent flames. Such measurements have been made in a lean premixed combustor under stable and unstable operating conditions and have shown to be in good agreement with OH^* chemiluminescence measurements of the rate of heat release.[75]

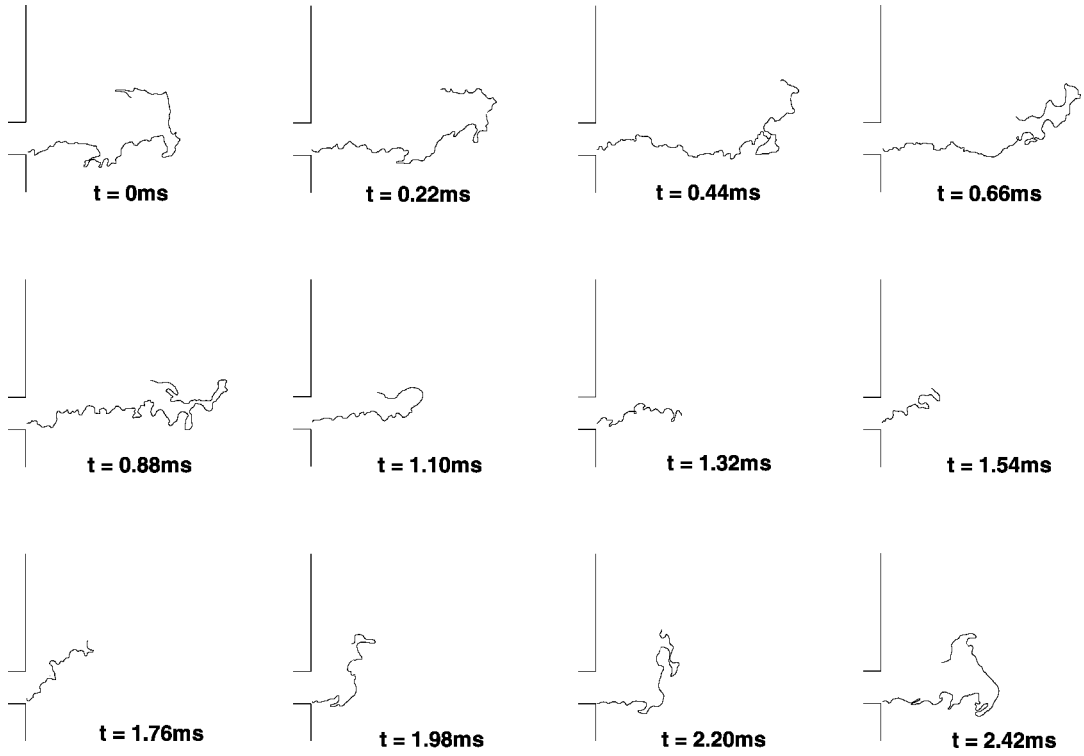

Fig. 24 Sequence of digitized flame surfaces over one period of unstable combustion.

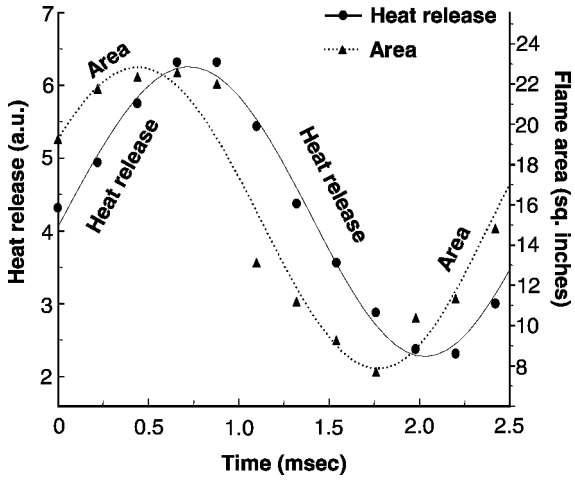

Fig. 25 Variation of flame area and heat release with time during one period of unstable combustion.

Conclusions

Chemiluminescence emission-, infrared absorption-, and laser-induced fluorescence-based measurement techniques, when combined with phase-synchronized pressure fluctuation measurements, can be used to obtain a detailed characterization of unstable combustion and the underlying mechanisms of unstable combustion in lean premixed gas turbine combustors.

Chemiluminescence emission measurements can be used to monitor fluctuations in the flame's overall heat release, as well as fluctuations in the flame's structure during unstable combustion. Simultaneous measurements of overall heat release and pressure fluctuations provide information related to the overall system gain and damping. Phase-synchronized chemiluminescence flame structure measurements reveal the spatial and temporal evolution of the flame's heat release and provide insight regarding the phenomenology of an instability, such as showing evidence of flame–vortex interaction or periodic extinction and reignition. Simultaneous flame structure measurements and pressure measurements can be used to calculate the Rayleigh index distribution from which regions of gain and damping can be identified.

Infrared absorption can be used to measure the frequency and magnitude of equivalence ratio fluctuations at the entrance to the combustor during unstable combustion. Such measurements, when combined with simultaneous pressure and overall heat release fluctuation measurements, can be used to quantify the role of feed system coupling and to assess the effectiveness of control strategies for suppressing the instability.

Laser-induced fluorescence measurements can be used to characterize fuel–air mixing and the resultant fuel distribution at the inlet to the combustor. Phase-synchronized OH PLIF measurements can be used to obtain detailed information about the flame structure and its evolution during an instability. For example, OH PLIF measurements can be used to calculate the flame area, which, when combined with simultaneous heat release and pressure fluctuation measurements, provides quantitative information regarding the role of flame area changes during an instability.

The detailed information that can be obtained with these measurement techniques is critical to improving our understanding of unstable combustion, to the formulation and validation of reduced-order models of unstable combustion, and to the identification and optimization of strategies for suppressing unstable combustion.

Acknowledgments

The authors are grateful for the financial support provided by the Advanced Gas Turbine Systems Research Program of the Department of Energy, the Air Force Office of Scientific Research, the Office of Naval Research, General Electric Company, Pratt & Whitney, Siemens Westinghouse, Solar Turbines, and United Technologies Research Center. The authors would like to acknowledge a number of graduate students and postdoctoral students who contributed to the work presented in this paper, including R. Bandaru, S. Berksoy, K. Kim, S. Miller, L. Preston, J. Samperio, D. Simons and K. K. Venkataraman.

References

[1] Oran, E. S., and Gardner, J. H., "Chemical-Acoustic Interactions in Combustion Systems," *Progress in Energy and Combustion Science*, Vol. 11,

No. 4, 1985, pp. 253–276.

[2]Candel, S. M., and Poinsot, T. J., "Interactions Between Acoustics and Combustion," *Proceedings of the Inst. of Acoustics*, Inst. of Acoustics, St. Albans, Vol. 10, 1988, pp. 103–153.

[3]Keller, J. J., "Thermoacoustic Oscillations in Combustion Chambers of Gas Turbines," *AIAA Journal*, Vol. 33, No. 12, 1995, pp. 2280–2287.

[4]Dowling, A. P., "The Calculation of Thermoacoustic Oscillations, *Journal of Sound and Vibration*, Vol. 180, No. 4, 1995, pp. 557–581.

[5]Poinsot, T., Trouve, A., Veynante, D., Candel, S., and Esposito, E., "Vortex-Driven Acoustically Coupled Combustion Instabilities," *Journal of Fluid Mechanics*, Vol. 177, 1987, pp. 265–292.

[6]Schadow, K. C., Gutmark, E., Parr, T. P., Parr, D. M., Wilson, K. J., and Crump, J. E., "Large-Scale Coherent Structures as Drivers of Combustion Instability," *Combustion Science and Technology*, Vol. 64, 1989, pp. 167–186,

[7]Straub, D., Richards, G., Yip, M. J., Rogers, W. A., and Robey, E. H., "Importance of Axial Swirl Vane Location on Combustion Dynamics for Lean Premix Fuel Injectors," AIAA Paper 98-3909, July 1998.

[8]Richards, G. A., and Janus, M. C., "Characterization of Oscillations During Premixed Gas Turbine Combustion," *Journal of Engineering for Gas Turbines and Power*, Vol. 120, No. 2, 1998, pp. 294–302.

[9]Lieuwen, T., and Zinn, B. T., "The Role of Equivalence Ratio Oscillations in Driving Combustion Instabilities in Low NO_x Gas Turbines," *Proceedings of the Combustion Institute*, Vol. 27, 1998, pp. 1809–1816.

[10]Lee, J. G., Kim, K., and Santavicca, D. A., "Measurement of Equivalence Ratio Fluctuation and Its Effect in Heat Release During Unstable Combustion," *Proceedings of the Combustion Institute*, Vol. 28, 2000, pp. 415–421.

[11]Lieuwen, T., Torres, H., Johnson, C., and Zinn, B. T., "A Mechanism of Combustion Instability in Lean Premixed Gas Turbine Combustors," *ASME Transactions*, Vol. 123, 2001, pp. 182–189.

[12]Lieuwen, T. C., Experimental Investigation of Limit-Cycle Oscillations in an Unstable Gas Turbine Combustor," *Journal of Propulsion and Power*, Vol. 18, No. 1, 2002, pp. 61–67.

[13]Lieuwen, T. C., "Statistical Characteristics of Pressure Oscillations in a Premixed Combustor," *Journal of Sound and Vibration*, Vol. 260, No. 1, 2003, pp. 3–17.

[14]Harrje, D. T., and Reardon, F. H. (eds.), "Liquid Propellant Rocket Combustion Instability," NASA SP-194, 1972, pp. 467, 468.

[15]Lieuwen, T., and Zinn, B. T., "On the Experimental Determination of Combustion Process Driving in an Unstable Combustor," *Combustion Science and Technology*, Vol. 157, No. 1, 2000, pp. 111–127.

[16]Lee, D. H., and Lieuwen, T., "Acoustic Nearfield Characteristics of a Conical, Premixed Flame," *Journal of the Acoustic Society of America*, Vol. 113, No. 1, 2003, pp. 167–177.

[17]Richards, G. A., Straub, D. L., and Robey, E. H., "Passive-Active Control of Combustion Oscillations," Spring Meeting of the Central States Section of the Combustion Inst., 2002.

[18]Lee, J. G., Kim, K., and Santavicca, D. A., "A Study of the Role of Equivalence Ratio Fluctuation During Unstable Combustion in a Lean Premixed Combustor," AIAA Paper 2002-4015, July 2002.

[19]Gaydon, A. G., *Spectroscopy of Flames*, Chapman and Hall, London, 1974.

[20]Gaydon, A. G., and Wolfhard, H. G., *Flames, Their Structure, Radiation and Temperature*, Chapman and Hall, London, 1979.

[21]Miller, S. A., "Development of a Flame Chemiluminescence Probe for Determination of Primary Zone Equivalence Ratio in Gas Turbine Combustors," M.S. Thesis, Dept. of Mechanical and Nuclear Engineering, The Pennsylvania State Univ., University Park, PA, Aug. 1999.

[22]John, R., and Summerfield, M., "Effect of Turbulence on Radiation Intensity From Propane–Air Flames," *Jet Propulsion*, Vol. 27, 1957, pp. 169–178.

[23]Clark, T., "Studies of OH, CO, CH and C_2 Radiation From Laminar and Turbulent Propane–Air and Ethylene–Air Flames," NACA TN 4266, No. 4, 1958.

[24]Diederichsen, J., and Gould, R. D., "Combustion Instability: Radiation from Premixed Flames of Variable Burning Velocity," *Combustion and Flame*, Vol. 9, 1965, pp. 25–31.

[25]Hurle, I. R., Price, R. B., Sugden, T. M., Thomas, R. R. S., and Thomas, A., "Sound Emission from Open Turbulent Premixed Flames," *Proceedings of the Royal Society of London, Series A: Mathematical and Physical Science*, Vol. 303, 1968, pp. 409–427.

[26]Price, R., Hurle, I., and Sugden, T., "Optical Studies of the Generation of Noise in Turbulent Flames," *Proceedings of the Combustion Institute*, Vol. 12, 1968, pp. 1093–1102.

[27]Hedge, E. G., Reuter, D., Daniel, B. R., and Zinn, B. T., "Flame Driving of Longitudinal Instabilities in Dump Type Ramjet Combustors," *Combustion Science and Technology*, Vol. 55, 1987, pp. 125–138.

[28]Langhorne, P. J., "Reheat Buzz: An Acoustically Coupled Combustion Instability. Part 1. Experiment," *Journal of Fluid Mechanics*, Vol. 193, 1988, pp. 417–443.

[29]Samaniego, J. M., Yip, B., Poinsot, T., and Candel, S., "Low-Frequency Combustion Instability Mechanisms in a Side-Dump Combustor," *Combustion and Flame*, Vol. 94, No. 4, 1993, pp. 363–380.

[30]Shih, W.-P., Lee, J. G., and Santavicca, D. A., "Stability and Emissions Characteristics of a Lean Premixed Gas Turbine Combustor," *Proceedings of the Combustion Institute*, Vol. 26, 1996, pp. 2771–2778.

[31]Bandaru, R. V., Miller, S., Lee, J. G., and Santavicca, D. A., "Sensors for Measuring Primary Zone Equivalence Ratio in Gas Turbine Combustors," Proceedings of SPIE (Society of Photo-Optical Instrumentation Engineers), Vol. 3535, The International Society for Optical Engineering, Bellingham, WA, 1991, pp. 104–114.

[32]Broda, J. C., Seo, S., Santoro, Shirhattakar, G., and Yang, V., "An Experimental Study of Combustion Dynamics of a Premixed Swirl Injector," *Proceedings of the Combustion Institute*, Vol. 27, 1998, pp. 1849–1856.

[33]Venkataraman, K. K., Preston, L. H., Simons, D. W., Lee, B. J., Lee, J. G., and Santavicca, D. A., "Mechanism of Combustion Instability in a Lean Premixed Dump Combustor," *Journal of Propulsion and Power*, Vol. 15, No. 6, 1999, pp. 909–918.

[34]Haber, L., Vandsberger, U., Saunders, W., and Khanna, V., "An Examination of the Relationship Between Chemiluminescence Light Emissions and Heat Release Rate Under Non-Adiabatic Conditions," International Gas Turbine Inst., Paper 2000-GT-0121, 2000.

[35]Ikeda, Y., Kojima, J., Nakajima, T., Akamatsu, F., and Katsuki, M., "Measurement of the Local Flame-Front Structure of Turbulent Premixed Flames by Local Chemiluminescence," *Proceedings of the Combustion Institute*, Vol. 28, 2000, pp. 343–350.

[36]Lieuwen, T., and Neumeier, Y., "Nonlinear Pressure-Heat Release Transfer Function Measurements in a Premixed Combustor," *Proceedings of the Combustion Institute*, Vol. 29, 2002, pp. 99–105.

[37]Paschereit, C. O., and Gutmark, E. J., "Enhanced Performance of a Gas-Turbine Combustor Using Miniature Vortex Generators,"*Proceedings of the Combustion Institute*, Vol. 29, 2002, pp. 123–129.

[38]Bellows, B. D., Zhang, Q., Neumeier, Y., Lieuwen, T., and Zinn, B. T., "Forced Response Studies of a Premixed Flame to Flow Disturbances in a Gas Turbine Combustor," AIAA Paper 2003-824, Jan. 2003.

[39]Samaniego, J. M., Egolfopoulos, F. N., and Bowman, C. T., "CO_2^* Chemiluminescence in Premixed Flames," *Combustion Science and Technology*, Vol. 109, 1995, pp. 183–203.

[40]Dandy, D., and Vosen, S., "Numerical and Experimental Studies of Hydroxyl Radical Chemiluminescence in Methane-Air Flames," *Combustion Science and Technology*, Vol. 82, 1992, pp. 131–150.

[41]Najm, H. N., Paul, P. H., Mueller, C. J., and Wyckoff, P. S., "On the Adequacy of Certain Experimental Observables as Measurements of Flame Burning Rate," *Combustion and Flame*, Vol. 113, 1998, pp. 312–332.

[42]Najm, H. M., Knio, O. M., Paul, P. H., and Wyckoff, P. S., "A Study of Flame Observables in Premixed Methane-Air Flames," *Combustion Science and Technology*, Vol. 140, 1998, pp. 369–403.

[43]Dowling, A. P., "Nonlinear Self-Excited Oscillations of a Ducted Flame," *Journal of Fluid Mechanics*, Vol. 346, 1997, pp. 271–290.

[44]Peracchio, A. A., and Proscia, W. M., "Nonlinear Heat-Release/Acoustic Model for Thermoacoustic Instability in Lean Premixed Combustors," American Society of Mechanical Engineers, ASME Paper 98-GT-269, 1998.

[45]Dasch, C. J., "One-Dimensional Tomography: A Comparison of Abel, Onion-Peeling, and Filtered Backprojection Methods," *Applied Optics*, Vol. 31, No. 8, 1992, pp. 1146–1152.

[46]Kim, K., Lee, J. G., and Santavicca, D. A., "Optimization of the Spatial and Temporal Fuel Distribution for Active Control of Combustion Dynamics in Lean Premixed Combustors," AIAA Paper 2002-4024, July 2002.

[47]Mallard, W. G., and Gardiner, W. C., Jr., "Absorption of the 3.39 μm He-Ne Laser Line by Methane from 300 to 2400K," *Journal of Quantitative Spectroscopy and Radiative Transfer*, Vol. 20, No. 2, 1978, pp. 135–149.

[48]Philippe, L. C., and Hanson, R. K., "Laser Diode Wavelength-Modulation Spectroscopy for Simultaneous Measurement of Temperature, Pressure and Velocity in Shock-Heated Oxygen Flows," *Applied Optics*, Vol. 32, No. 30, 1993, pp. 6090–6103.

[49]Yoshiyama, S., Hamamoto, Y., Tomita, E., and Minami, K., "Measurement of Hydrocarbon Fuel Concentration by Means of Infrared Absorption Technique with 3.39 μm He-Ne Laser," *Japanese Society of Automotive Engineering (JSAE) Review*, Vol. 17, No. 4, 1996, pp. 339–345.

[50]Mongia, R. K., Tomita, E., Hsu, F. K., Talbot, L., and Dibble, R. W., "Use of an Optical Probe for Time-Resolved *In situ* Measurement of Local Air-to-Fuel Ratio and Extent of Fuel Mixing with Applications to Low NOx Emissions in Premixed Gas Turbines," *Proceedings of the Combustion Institute*, Vol. 26, 1996, pp. 2749–2755.

[51]Koenig, M., and Hall, M. J., "Measurements of Local In-Cylinder Fuel Concentration Fluctuations in a Firing SI Engine," Society of Automotive Engineers, SAE Paper 971644, 1997.

[52]Wehe, S. D., Baer, D. S., and Hanson, R. K., "Tunable Diode-Laser Absorption Measurements of Temperature, Velocity and H2O in Hypersonic Flows," AIAA Paper 97-3267, July 1997.

[53]Mihalcea, R. M., Baer, D. S., and Hanson, R. K., "Diode-Laser Sensor for Measurements of CO, CO2 and CH4 in Combustion Flows," *Applied Optics*, Vol. 36, No. 33, 1997, pp. 8745–8752.

[54]Seitzman, J. M., Tamma, R., and Vijayan, R., "Infrared Absorption Based Sensor Approaches for High Pressure Combustion," AIAA Paper 97-0318, Jan. 1997.

[55]Mongia, R. K., Dibble, R. W., and Lovett, J., "Measurement of Air–Fuel Ratio Fluctuations Caused by Combustor Driven Oscillations," American Society of Mechanical Engineers, ASME Paper 98-GT-304, 1998.

[56]Mihalcea, R. M., Baer, D. S., and Hanson, R. K., "Advanced Diode Laser Absorption Sensor for In-Situ Combustion Measurements of CO_2, H_2O and Gas Temperature," *Proceedings of the Combustion Institute*, Vol. 27, 1998, pp. 95–101.

[57]Mongia, R., Torres, J., Dibble, R., Lee, D., Anderson, T., and Sowa, W., "Fast Response Extraction Probe for Measurement of Air-Fuel Ratio Fluctuations in Lean Premixed Combustors," American Society of Mechanical Engineers, ASME Paper 99-GT-277, 1999.

[58]Ebert, V., Fernholz, T., Giesemann, C., Pitz, H., Teichert, H., and Wolfrum, J., "Simultaneous Diode-Laser-Based In-Situ-Detection of Multiple Species and Temperature in a Gas-Fired Power-Plant," *Proceedings of the Combustion Institute*, Vol. 28, 2000.

[59]Webber, M. E., Wang, J., Sanders, S. T., Baer, D. S., and Hanson, R. K., "In-situ Combustion Measurements of CO, CO2, H2O and Temperature Using Diode Laser Absorption Sensors," *Proceedings of the Combustion Institute*, Vol. 28, 2000, pp. 407–413.

[60]Eckbreth, A. C., *Laser Diagnostics for Combustion Temperature and Species*, 2nd Ed., Gordon and Breach, New York, 1996.

[61]Nguyen, Q.-V., and Paul, P. H., "The Time Evolution of a Vortex-Flame Interaction Observed via Planar Imaging of CH and OH," *Proceedings of the Combustion Institute*, Vol. 26, 1996, pp. 357–364.

[62]Seitzman, J. M., Kychakoff, G., and Hanson, R. K., "Instantaneous Temperature Field Measurements Using Planar Laser-Induced Fluorescence," *Optics Letters*, Vol. 10, No. 9, 1985, pp. 439–441.

[63]Hanson, R. K., "Combustion Diagnostics: Planar Flowfield Imaging," *Proceedings of the Combustion Institute*, Vol. 21, 1986, pp. 1677–1691.

[64]Hanson, R. K., "Planar Laser-Induced Fluorescence Imaging," *Journal of Quantitative Spectroscopy and Radiative Transfer*, Vol. 40, No. 3, 1988, pp. 343–362.

[65]Pringsheim, P., *Fluorescence and Phosphorescence*, Interscience, New York, 1949.

[66]Berlman, I. B., *Handbook of Fluorescence Spectra of Aromatic Molecules,* Academic Press, New York, 1971.

[67]Lozano, A., Yip, B., and Hanson, R. K., "Acetone: A Tracer for Concentration Measurements in Gaseos Flows by Planar Laser-Induced Fluorescence," *Experiments in Fluids*, Vol. 13, 1992, pp. 369–376.

[68]Thurber, M. C., and Hanson, R. K., "Simultaneous Imaging of Temperature and Mole Fraction Using Acetone Planar Laser Induced Fluorescence," *Experiments in Fluids*, Vol. 30, 2001, pp. 93–101.

[69]Koch, J. D., and Hanson, R. K., "Ketone Photophysics for Quantitative PLIF Imaging," AIAA Paper 2000-0413, Jan. 2001.

[70]Thurber, M. C., and Hanson, R. K., "Pressure and Composition Dependence of Acetone Laser-Induced Fluorescence with Excitation at 248, 266 and 308 nm," *Applied Physics B*, Vol. 69, No. 3, 1999, pp. 229–240.

[71]Samperio, J. L, Lee, J. G., and Santavicca, D. A., "Characterization of the Effect of Inlet Operating Conditions on the Performance of Lean Premixed Gas Turbine Combustors," AIAA Paper 2003-0825, Jan. 2003.

[72]Lee, J. G., and Santavicca, D. A. "Fiber-Optic Probe for Laser-Induced Fluorescence Measurements of the Fuel–Air Distribution in Gas-Turbine Combustors," *Journal of Propulsion and Power*, Vol. 13, No. 3, 1997, pp. 384–387.

[73]Venkataraman, K. K., Lee, J. G., and Santavicca, D. A., "The Role of Flame Stretch During Unstable Combustion in a Lean Premixed Combustor," *Journal of Propulsion and Power*, (submitted for publication).

[74]Venkataraman, K. K., "An Investigation of the Instability Mechanism in Lean Premixed Dump Combustors," Ph.D. Dissertation, Dept. of Mechanical and Nuclear Engineering, Pennsylvania State Univ., University Park, PA, 2000.

[75]Lee, S.-Y., Seo, S., Broda, J. C., Pal, S., and Santoro, R. J., "An Experimental Estimation of Mean Reaction Rate and Flame Structure During Combustion Instability in a Lean Premixed Gas Turbine Combustor," *Proceedings of the Combustion Institute*, Vol. 28, 2000, pp. 775–782.

[76]Santhanam, V., Knopf, F. C., Acharya, S., and Gutmark, E., "Fluorescence and Temperature Measurements in an Actively Forced Swirl-Stabilized Spray Combustor," *Journal of Propulsion and Power*, Vol. 18, 2002, pp. 855–865.

[77]Peters, N., "Laminar Flamelet Concepts in Turbulent Combustion," *Proceedings of the Combustion Institute*, Vol. 21, 1986, pp. 1232–1250.

[78]Buschmann, A., Dinkelacker, F., Schäfer, T., and Wolfrum, J., "Measurement of the Instantaneous Detailed Flame Structure in Turbulent Premixed Combustion," *Proceedings of the Combustion Institute*, Vol. 26, 1996, pp. 437–445.

[79]Dunkelacker, F., Soika, A., Most, D., Hofman, D., Leipertz, A., Polifke, W., and Döbbeling, K., "Structure of Locally Quenched Highly Turbulent Lean Premixed Flames," *Proceedings of the Combustion Institute*, Vol. 27, 1998. pp. 857–865.